

3. FISSION PRODUCT TRANSPORT IN TRISO-COATED PARTICLE FUELS

3.1 Introduction

The purpose of this section is to discuss the potential phenomena (generalized to the term “factors” in this report) associated with the transport of fission products in TRISO-coated particle fuel. Fission product transport in the coated particle is a key component of the source term calculation for the high-temperature gas-cooled reactor and is very useful for evaluation of factors identified by the PIRT panel. TRISO-coated particle fuel is a complex fuel form from the perspective of fission product modeling. The multiple layers, the chemical state of the fission products, the different mechanisms responsible for gaseous and metallic fission product transport in each layer, and the projected high burnups and fast neutron fluences make the modeling of fission product transport challenging. Sections 3.2 through 3.5 discuss fission product transport in the TRISO-coated particle fuel layer by layer. Each section includes a review of the existing database for transport in the layer, discusses potential mechanisms responsible for the transport, and presents results of preliminary scoping calculations for the transport in the layer. In Section 3.6, a simplified integrated transport model is presented and some simple sensitivity results are discussed. These results are used to provide a better understanding of the individual sub-factors associated with the fission product transport factors identified by the PIRT panel. In Section 3.7, these factors are defined and the rationale for the selection of these factors to capture the overall complexity of fission product transport is discussed. Section 3.8, summarizes our findings.

3.2 The Fuel Kernel

Fission product transport in the kernel is complex. Important mechanisms (i.e., factors) include recoil, diffusion of fission products to grain boundaries, vaporization, and transport through the interconnected porosity of the kernel to the surface of the kernel and chemical reaction at the boundary of the kernel. These processes are functions of burnup and temperature and thus change over the life of the fuel.

3.2.1. Recoil

Recoil from the kernel can be estimated using the following equation:

$$(RF)_{\text{recoil}} = 0.25 [r_k^3 - (r_k - d)^3] / r_k^3$$

where RF is the release due to recoil, r_k is the radius of the fuel kernel and d is the average fission fragment range. The average fission fragment ranges are calculated for a given fuel composition from experimental data [3-1]. Based on fission energies of 107 MeV for krypton and 72 MeV for xenon, the average krypton range is 5.8 microns and the average xenon range is 4.1 microns in UO_2 with a density of 10.5 g/cm^3 . Thus, for a 500-micron kernel, the recoil release fraction is about 1.5%. For a 350-micron kernel, the recoil release fraction is about 2%.

3.2.2. Chemical Reaction at the Fuel Kernel Boundary

Fuel kernels are chemically reactive with the surrounding graphite. This is especially true for UO_2 kernels. There will be some reaction of the graphite with the kernels to produce surface layers of uranium carbide or oxycarbide and carbon monoxide (CO). The structure of uranium carbide is different from the structure of uranium dioxide. The reaction is not topotactic¹ and restructuring of the surface material takes place. The restructuring causes the material to evolve toward a more nearly equilibrium state by expelling to its surfaces some fractions of the impurities including fission products. Because these fission products are moved during the recrystallization process to the exposed surfaces of the fuel kernel, they are usually considered to be released from the kernel. Because of the temperature dependence of the reaction of graphite with the kernel, reaction release of fission products can become progressively more important as temperatures increase.

During normal operations, kinetics of reaction limit the rate of fission product release from fuel kernels by reaction with the graphite. Out-of-pile studies of the reaction kinetics are of limited use because the effects of graphite irradiation is not accounted for. Irradiation of the graphite creates dislocations of the graphite structure that are energetic and more reactive than unirradiated graphite toward the fuel kernel.

3.2.3. Booth Diffusion

Far more important than either recoil or reaction as transport mechanisms of release (especially under accident conditions) is the conventional release process of fission product diffusion through grains to the grain boundaries and subsequent transport through the interconnected porosity. This mechanism has been studied extensively in the context of light water reactor fuel behavior. The Booth diffusion model has been used to estimate the release of fission gases via these mechanisms and has been used to describe fission product release from the kernel. The release fraction is given by [3-2]:

$$FR = 1 - \left(\frac{6}{D't} \right) \sum_{n=1}^{\infty} [1 - \exp(-n^2 \pi^2 D't)] / [n^4 \pi^4]$$

where D' is the reduced diffusivity, which is equal to D/a^2 and t , is equal to time. The two key parameters in the model are a , the effective radius for diffusion, and D the diffusion coefficient. This equation has been used to establish reduced diffusivities (D'/a^2) from integral irradiation and high temperature experiments. This approach produces a reduced diffusion coefficient that is time-averaged and volume-weighted. The formulation for diffusion coefficients by Turnbull, which accounts for intrinsic, athermal and radiation-enhanced diffusion, is believed to be the most accurate for UO_2 . [3-3,3-4] The definition of the effective radius is usually taken to be the grain size of the UO_2 .

¹ topotactic transition: a transition in which the crystal lattice of the product phase shows one or more crystallographically equivalent, orientational relationships to the crystal lattice of the parent phase.

There are several limitations with the Booth model:

- a. The original Booth model was used to describe gas release from a fuel grain and not a fuel kernel or fuel pellet per se where the gas phase transport in the interconnected porosity is also important.

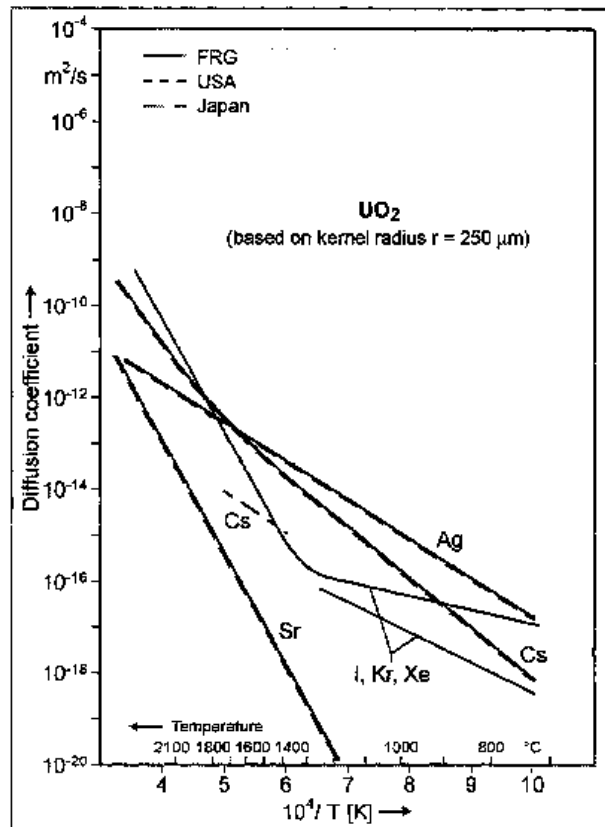


Figure 3-1 Comparison of measured diffusivities of fission gases and some fission metals in UO_2 kernels of coated particle fuel [3-5]

- b. The use of the Booth model makes it difficult to accurately capture the effect of burnup on the microstructural changes in the kernel and the subsequent impact on release.²

² The variability in the reduced diffusivity derived from the integral release measurements may be quite large when the morphology changes in the kernel with burnup are considered. Low releases are expected at low burnup. At moderate to high burnup, the restructuring of the kernel can be extensive resulting in large release. This is a key shortcoming in using such a simple model to account for very complex fuel microstructural evolution and attendant fission product release.

- c. The release of some of the metallic fission products, which tend to form nodules along grain boundaries in the fuel (e.g., Ru, Mo, Tc, Pd), is not governed by this classic diffusion mechanism.

Despite these shortcomings, many researchers have correlated or “force-fitted” release measurements to an “effective Booth model.” For coated particle fuels, reduced diffusivities exist for the fission gases and some fission metals like cesium, silver, and strontium. The effects of changes in the microstructure with burnup are not directly accounted for but are implicit in the values used for D' . Figure 3-1 is a plot of the values of D measured on UO_2 coated particles by the Germans (assuming $a = 250$ microns) [3-5] and they form the baseline to be used for scoping analysis presented here. No diffusivity data exist for noble fission metals like Ru, Mo, Tc, and Pd. Similar data do not exist for UCO and thus UO_2 values are used in the interim.

This effective Booth model has been used with the measured diffusivities for UO_2 fuel to determine the impact of time (i.e., burnup) and temperature on the release of fission gas, cesium, silver and strontium from a 500-micron UO_2 kernel. Three specific calculations have been performed:

- A three-year 900°C irradiation, typical of the average exposure of a UO_2 coated particle in a prismatic reactor
- A three-year 1200°C irradiation, typical of the peak exposure of a UO_2 coated particle in a prismatic reactor
- A three-year 600 to 1200°C ten cycle exposure typical of peak exposure of a UO_2 coated particle in a pebble bed reactor.

The resultant fission product releases are shown in Figures 3-2, 3-3 and 3-4. The results indicate that time at temperature is important and can make a difference in the release fraction of the fission products from the kernel. Given the exponential nature of the diffusivities, as expected the release is dominated by the time at high temperature.

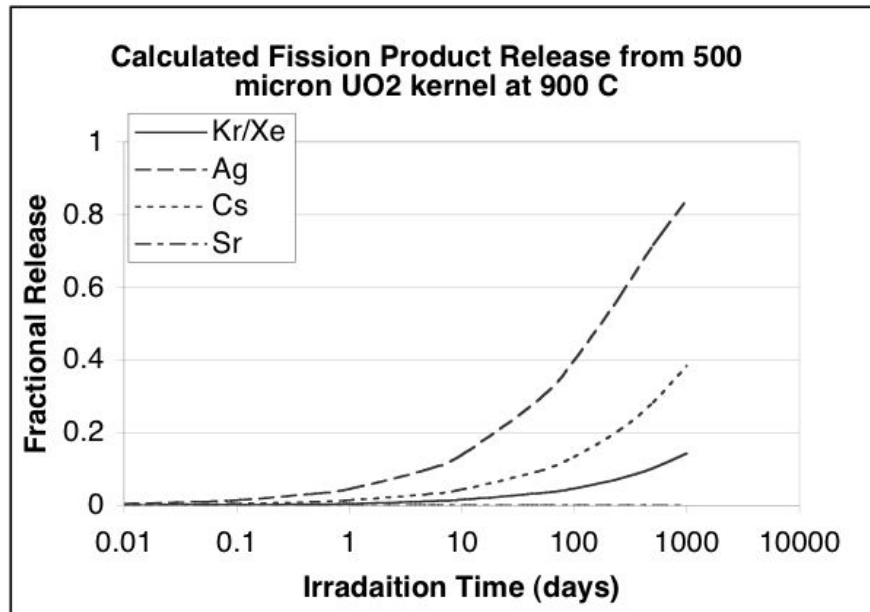


Figure 3-2 Calculated fission product release from 500 micron UO₂ kernel at 900°C

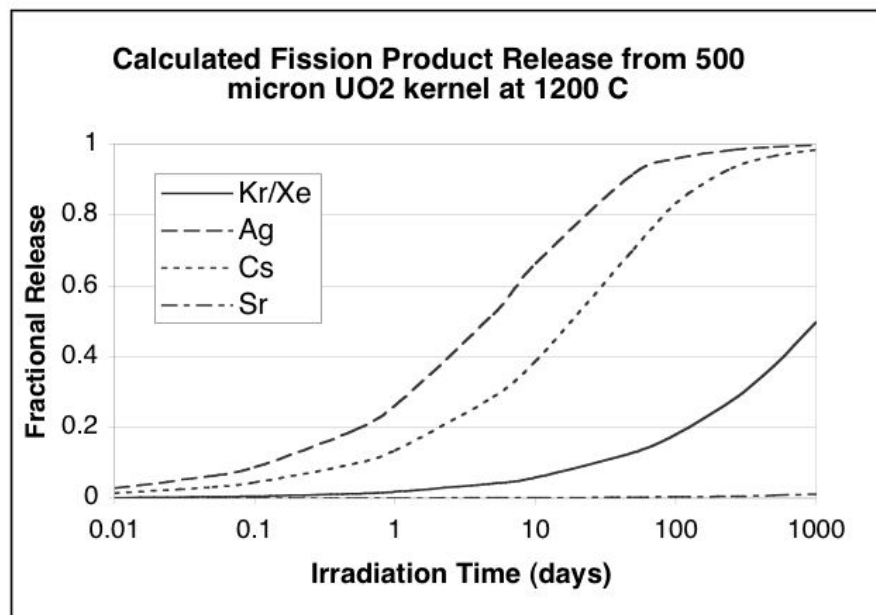


Figure 3-3 Calculated fission product release from 500 micron UO₂ kernel at 1200°C

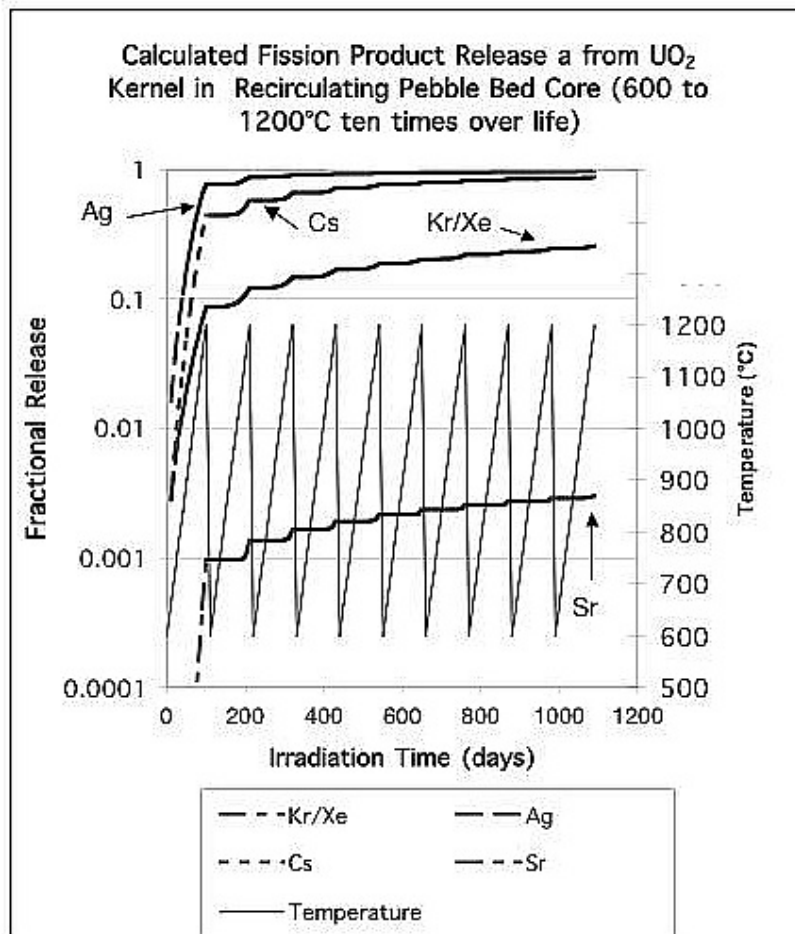


Figure 3-4 Influence of cyclic temperature in a pebble bed reactor on fission product release from a 500 micron UO_2 kernel

3.2.4. Vaporization: Fission Product Chemical Form

The estimation of fission product transport through the layers of coated particle fuel requires an understanding of the gas-phase speciation of fission products released from the fuel. The chemical environment of the fuel particle will be reducing and different than exists at any point in the release of fission products for light water reactor cores. The speciation will be sensitive to the reducing conditions. Furthermore, graphite and carbon monoxide produced by the reaction of graphite with oxygen liberated by the fission process can affect the speciation.

Speciation in terms of elemental vapor species and oxide vapor species can be determined with existing thermochemical data. There are, however, possibilities for vapor species that are not as well known forming in the environment of the coated particle fuels. These include impurities left from the manufacturing process such as HCl , which can affect speciation by the formation of chlorides of the fission products.

Chlorides are typically volatile. There are recognized databases on the thermochemical properties of condensed chlorides of most of the fission products. Data bases on vapor species, especially monochloride and dichloride vapor species or oxychloride vapor species, have not been as comprehensively compiled though data are available.

More exotic species in the sense that they are less familiar in the analysis of light water reactor accidents include vapor phase carbide species. There is also evidence for the formation of the vapor phases of BaC, SrC, ZrC and RuC. Again, the necessary review of the literature to produce a well-founded compilation of vapor-phase carbides has not been done.

Another class of species that is not well known in a thermochemical sense is the vapor phase carbonyls. Metal carbonyls $(\text{CO})_n$ are well known chemically and used as precursors for the synthesis of organometallics. Notable species include $\text{Ni}(\text{CO})_4$ and $\text{Fe}(\text{CO})_5$ and carbonyls of many other transition elements. These, however, are not the species of primary interest in relation to the transport of fission products in coated particle fuels at the high temperatures arising in reactor accidents, because they are not radiologically important. In these conditions vapor species that are monocarbonyls (MCO) and dicarbonyls ($\text{M}(\text{CO})_2$) are likely to be of more interest [3-[6]. Thermochemical data for such species are not abundant simply because there has been little incentive to look for and characterize such species. This, however, does not mean that the species are unimportant in the particular situation of interest here. (The level of knowledge about vapor phase carbides and carbonyls is similar to that of vapor phase hydroxides 50 years ago. Their existence is not well established, but they proved important for the understanding of factors other than fission product transport such as flames, magmatic processes and even some corrosion processes. They were eventually found by experiment and characterized.)

Speciation of fission products can become more complicated during accidents involving air and water intrusion. Then, in addition to the vapor species already mentioned, vapor phase hydrides, hydroxides, nitrides and even cyanides may affect the potential for fission product release.

The thermochemical data used for the calculation of the vapor speciation are enthalpies of formation and free-energy functions. The free-energy functions are usually calculated for vapor species from spectroscopic data, some of which can be very complicated for high molecular weight fission product species. Enthalpies of formation are usually derived from mass spectroscopic estimates of the temperature dependencies of vapor pressures or inferred from transpiration experiments. The uncertainties in the enthalpies of formation of vapor species can be as high as ± 20 kcal/mole.

3.3 The Buffer Layer

The buffer layer plays a role in the coated particle from the perspective of fission product transport. Depending on the specific irradiation conditions, the nature of the shrinkage and densification of the buffer establishes the initial condition for fission product

transport during irradiation and under accident conditions. The buffer is a porous carbon layer (~50% dense initially) whose function is to serve as a void volume for fission gases and act a material to absorb fission recoils and swelling of the fuel kernel. Sometimes the buffer cracks because of tangential stresses developed under irradiation. Because of the high porosity of the layer, it has the lowest conductivity of any layer in the coated particle and thus the largest temperature drop. Depending on the power produced in the kernel, the temperature gradient in the buffer may cause thermal (or Soret) fission product diffusion in the layer.

3.3.1. Thermal Behavior of the Buffer

For a first approximation, to calculate the internal temperature distribution in a coated particle it can be assumed that heat transfer is predominantly by radial heat conduction and that the outer boundary temperature of the fuel particle is uniform. In a spherical fuel kernel with uniform heat generation rate, q_f''' (W/m³), the steady state temperature rise from the center to the surface of the kernel is given by:

$$T_o - T_1 = - q_f''' r_1^2 / 6k_f$$

Where $T_o = T(0)$, $T_1 = T(r_1)$, r_1 = fuel kernel radius, and k_f = fuel kernel thermal conductivity. Ignoring heat generated in the buffer, the buffer temperature drop is given by:

$$T_1 - T_2 = q_f (r_2 - r_1) / 4\pi k_c r_1 r_2$$

Where r_2 = buffer outer radius, k_c = thermal conductivity of the buffer, and $q_f = (4/3)\pi r_1^3 q_f'''$ = thermal power generated in the fuel kernel. Assuming no gaps develop between layers, which can cause large temperature drops, similar equations apply to the temperature drops across other layers (IPyC, SiC, OPyC).

Table 3-1 presents the calculated temperature drop across each layer, and the layer's associated thermal properties for an average particle that generates ~ 62 mW of power, which is about the average power per particle in a pebble bed reactor core (PBR). Thus, for an average particle, the ~ 10 °K temperature drop across the buffer translates into ~ 100 °K/cm gradient across the layer.

Table 3-1 Calculated Temperature Drops Across Layers of a Coated Particle

	Outer Radius, μm	Conductivity k, W/m-K	Density ρ , kg/m ³	Heat Capacity C_p , J/kg-K	Temperature drop ΔT , °K Layer
UO₂ kernel	$r_1 = 250$	2.5	10960	332	3.92
Buffer (50% dense graphite)	$r_2 = 345$	0.5	1100	1.5	10.88
IPyC	$r_3 = 385$	4.0	1700	1.5	0.37
SiC	$r_4 = 420$	13.9	3200	0.5	0.07
OPyC	$r_5 = 460$	4.0	1700	1.5	0.26
				Total $\Delta T =$	15.5

Figure 3-5 plots the thermal gradient and the temperature drop across the buffer as a function of the power per particle for a standard 500 micron UO₂ German coated particle. As the power increases, significant thermal gradients can develop. These thermal gradients lead to increasing thermal stresses in the layer. The stresses in the buffer due to thermal gradients and densification, if high enough, could cause cracking of the buffer. Furthermore, high thermal gradients across the buffer ($> \sim 1000$ K/mm) can drive thermal diffusion (Soret effect) of fission products across the layer (see Section 3.3.3).

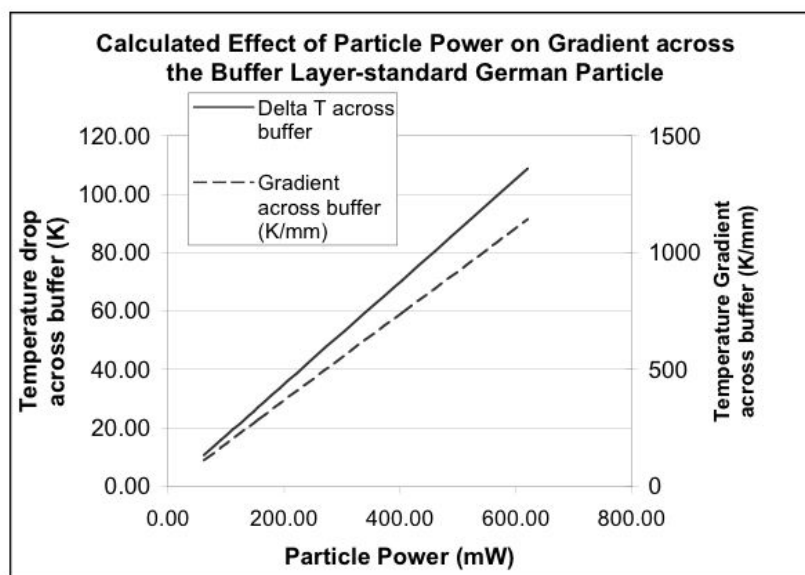


Figure 3-5 Calculated effect of particle power on temperature gradient and temperature drop across the buffer layer of a standard 500-micron UO₂ German particle

Figure 3-6 is a photomontage of different fuel particles irradiated under different power conditions. As shown in the figure, as the irradiation is accelerated the power in the particle is increased and the state of the buffer changes. The German LEU UO_2 particle from AVR shows very little change in the buffer after irradiation probably because of the low power being produced (the exact power history is not well known given the nature of pebble bed refueling). The LEU UCO particle from the HRB-14 irradiation shows a typical cracked buffer. These cracks can provide paths for more rapid fission product transport (see Section 3.3.2). The particle in HRB-15A is an example of more severe cracking of the buffer. The NPR-2 HEU UCO particle was irradiated at an accelerated factor of 10 compared to that expected in an HTGR. There is significant densification of the buffer on one side of the particle as the buffer shrank during the irradiation. (The cause of the excessive shrinkage in the NPR-2 photo is not known with certainty. It is the most accelerated irradiation ever conducted in the U.S. However, there may have been some chemical interactions between the kernel and the buffer that contributed to the final state shown in the micrograph).

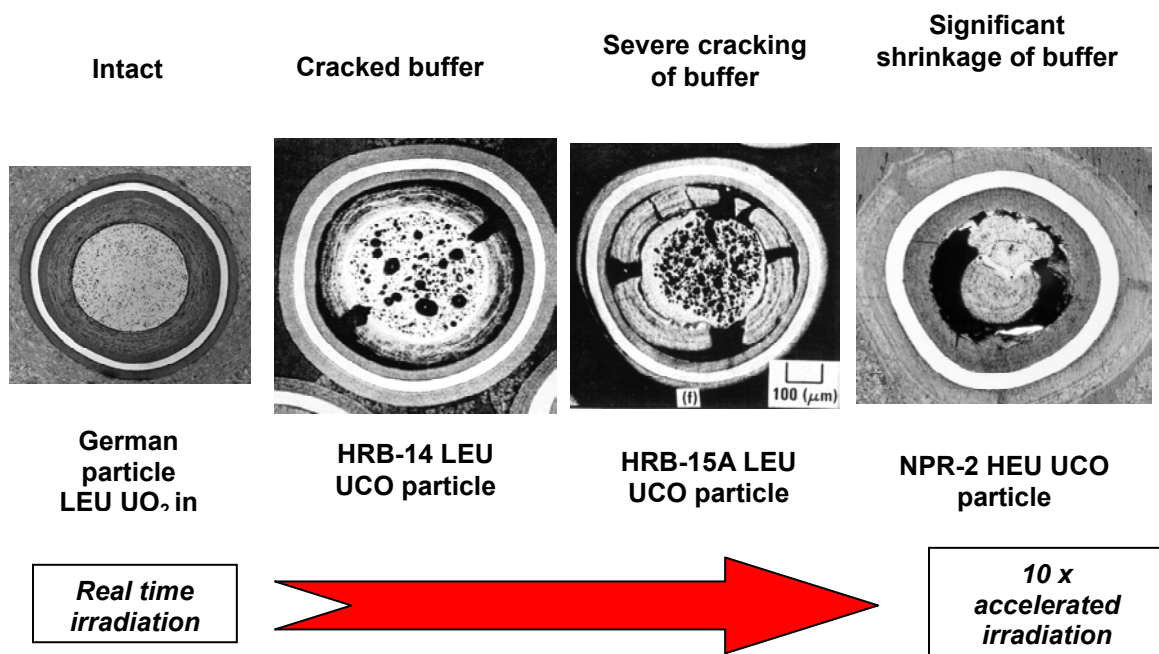
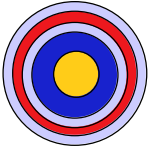
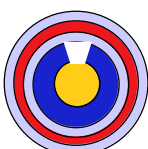
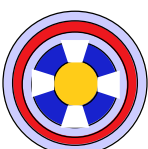
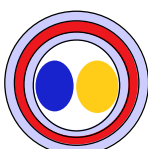


Figure 3-6 Different states of the buffer in coated particles following irradiation in the U.S.

Table 3-2 schematically presents this evolution of the buffer relative to particle power. The table describes possible locations where such powers might be found in a pebble bed reactor, in a prismatic reactor core or in an irradiation test reactor. In addition, the thermal gradient that develops across the buffer of a 500-micron UO_2 kernel has been estimated and some comments about the condition of the buffer are provided. (Note that the thermal gradients for a 350-micron kernel in a prismatic core would be about double that shown here for the same power level because of the smaller kernel size).

Table 3-2 Effects of Particle Power on the Buffer in Coated Particle Fuel

					
Description or location	PBMR low flux region; GT-MHR average	PBMR average	PBMR pebble and prismatic compact peak	Current prismatic irradiation limit	Very accelerated irradiations
Particle Power	25 to 40 mW	60 mW	100 mW	400 mW	500 to 5000 mW
Thermal gradient Across buffer (for 500 micron kernel)	< 50 K/mm	~ 100 K/mm	~ 250 K/mm	~ 750 K/mm	~ 900 to 9000 K/mm
Condition of buffer	Uniform shrinkage		Moderate tensile stress - some cracking	High tensile stress - many cracks	Excessive shrinkage; buffer and fuel side by side

3.3.2. Fission Product Transport in a Porous Medium

A complete description of fission gases and vapor in a porous media requires an understanding of multicomponent gas-phase mass transport. The multicomponent diffusion equation in the Chapman-Enskog [3-7] approximation is given by:

$$\left(\frac{P}{RT}\right)\vec{\nabla}x_i + \left(x_j - \frac{x_j m_j P / RT}{\rho}\right)\vec{\nabla} \ln P =$$

$$\sum_{j=1}^N \left(\frac{x_i \vec{N}_j - x_j \vec{N}_i}{[D_{*ij}]} \right) + \vec{\nabla} \ln T \sum_{j=1}^N \frac{1}{[D_{*ij}]} \left(\frac{x_i D_j^{(T)}}{m_j} - \frac{x_j D_i^{(T)}}{m_i} \right)$$

where:

- X_i = mole fraction vapor species i
- $[D_{*ij}]$ = first Chapman – Enskog approximation of the binary diffusion coefficient of species
- N_i = molar flux of species i (moles/cm²-g)
- P = total pressure
- R = gas constant
- T = temperature
- m_i = molecular weight of species i
- $D_i^{(T)}$ = thermal diffusion coefficient of species i

This formulation assumes that mass transfer occurs as a result of gradients in chemical composition (i.e., mole fractions), gradients in temperature³ (thermal diffusion or the Soret effect, see also Section 3.3.3) and gradients in pressure. (Note that as written above, the slip correction is not included in the pressure gradient coefficient. This slip correction, which accounts for relative velocity between the molecule and the surface when the characteristic size in the medium is on the order of the mean free path of the gas, has proven to be of some importance in the analysis of mass transport through graphite.) The dependence on pressure gradients can be important for mass transport across the SiC layer and is dominant in situations in which the porous medium has failed structurally and macroscopic cracks are present. The multicomponent diffusion equation, even in the absence of gradients in pressure and temperature, is difficult to solve. It also yields counter-intuitive results such as osmotic diffusion, barrier diffusion, and reverse diffusion [3-8]. These counter-intuitive results have generally been confirmed by experiment.

The solution of the binary form of the diffusion mass transport equation for transport of a vapor i in radial gradients in temperature and composition for a spherical shell with inner radius A and outer radius A + δ yields:

$$\frac{1}{A} \frac{dN_i}{dt} = \frac{PD_{*12}(T_b)}{RT_b^{1.5}} \frac{\Delta T}{2} \frac{(A + \delta)}{A\delta} \ln \left(\frac{1 - x_b}{1 - x_s} \right) \frac{1}{[T_b^{1/2} - T_s^{1/2}]} +$$

$$+ \frac{3\gamma D_{*12}(T_b)P(\Delta T)^2}{4R\Delta x T_b^{1.5}} \frac{(A + \delta)}{A\delta} \frac{[x_b^2 - x_s^2]}{[T_b^{1.5} - T_s^{1.5}]}$$

where the subscript b denotes conditions at the outer radius and the subscript s denotes conditions at the inner radius. γ is related to the thermal diffusion coefficients of the stagnant and mobile gases by:

$$\gamma = \frac{(RT)^2 \rho}{P^2 m_1 m_2} \frac{D_1^{(T)}}{D_{*12}}$$

When γ is greater than zero, the mobile gas moves toward cooler regions. From the above expression, it is evident that temperature gradients have a more global effect on the mass transport kinetics than just thermal diffusion.

The above development has been in terms of the Chapman-Enskog model because it is usually more familiar. Most investigators [3-9, 3-10] of mass transport through porous media have chosen to use the development by Grad (the so-called ‘13-moment’ method) because it allows the explicit consideration of the porous medium in the so-called ‘dusty

³ There are temperature dependencies in this equation, most notably the gas phase binary diffusion coefficients, which typically have a $T^{1.5}$ scaling at the accident temperatures considered here.

gas' approximation developed extensively by Mason and Malinauskas. The isothermal, binary diffusion (ternary if the immobile porous medium is considered) expression in this approximation is:

$$\vec{N}_i = -\frac{P}{RT} D_i(\text{eff}) \vec{\nabla} x_i + x_i \delta_i \vec{N} - x_i \gamma_i \frac{P}{RT} \frac{B_0}{\mu} \vec{\nabla} P$$

where:

$$\frac{1}{D_i(\text{eff})} = \frac{1}{D_i(\text{Kn})} + \frac{1}{D_{ij}(\text{eff})}$$

$$\delta_i = \frac{D_i(\text{eff})}{D_{ij}(\text{eff})}$$

$$\gamma_i = \frac{D_i(\text{eff})}{D_i(\text{Kn})}$$

$$\frac{1}{D(\text{Kn})} = \frac{x_i}{D_i(\text{Kn})} + \frac{x_j}{D_j(\text{Kn})}$$

$$D_i(\text{Kn}) = \frac{4}{3} K_0 \sqrt{8RT / \pi m_i}$$

$$D_{ij}(\text{eff}) = \frac{\varepsilon}{\tau} D_{*ij}$$

ε = porosity of the material

τ = tortuosity of pore network

Note that in some cases, it has been found necessary to introduce a slip correction for the coefficient of the pressure gradient term:

$$\frac{B_0}{\mu} + \frac{4}{3} K_0 \frac{\bar{v}}{P}$$

where \bar{v} is the mean molecular velocity.

The parameters in the equation are B_0 , the Poiseuille parameter, and the Knudsen parameter, K_0 . These parameters are properties of the porous material. An accurate evaluation of these parameters would require characterization of the material, which could be very difficult in the case of materials in coated particle fuel, or there would need to be some model of the material. For graphite, the following correlation has been established [3-11].

$$\log_{10} B_0 = -2.6891 + 1.2983 \log_{10} K_0$$

Given the large interconnected porosity in the buffer, the transport of gases in a porous medium (to describe the behavior of fission gases and vapors in the layer) has been examined. Pressure driven diffusion has been studied in porous mediums. References [3-12] and [3-13] provide a comprehensive overview of the subject. In all cases, the molar flux of material through the porous medium is a function of the pressure gradient

across the material. Three different regimes are traditionally considered depending on the mean free path of the gas relative to the characteristic size in the medium, or the Knudsen number ($Kn = \lambda/d_{pore}$, where λ is the mean free path). Characteristic sizes could range from nanopores in a material like an as fabricated buffer to microcracks as might be typical of a cracked buffer.

For $Kn > 1$, the mass transport behavior can be described using free molecular flow and the molar flux, given by:

$$\dot{N}_{Kn} = -\frac{D_{Kn}}{RT} \frac{\varepsilon_p}{\tau_{p,Kn}} \nabla p$$

$$D_{Kn} = (4/3) \bar{d}_{pore} \sqrt{RT/2\pi M}$$

where:

D_{Kn} = the Knudsen diffusivity,
 \bar{d}_{pore} = the average pore size in the medium,
 ε_p = the porosity of the medium
 $\tau_{p,Kn}$ = the tortuosity
 M = the molecular weight of the gas
 R = gas constant
 T = absolute temperature.

In the transition region, $0.01 < Kn < 1$, both viscous flow and diffusive flow are considered. They can be summed to determine the overall molar flux. Hence:

$$\dot{N} = \dot{N}_{vis} + \dot{N}_{diff}$$

$$\dot{N}_{diff} = -\frac{D_{Eff}}{RT} \frac{\varepsilon_p}{\tau_{p,Kn}} \nabla p$$

$$D_{Eff} = \left[\frac{1}{D_{Kn}} + \frac{1}{D_{12,gas}} \right]^{-1}$$

$$D_{Kn} = (4/3) \bar{d}_{pore} \sqrt{RT/2\pi M}$$

$$D_{12,gas} = \text{Chapman - Enskog - Theory}$$

$$\dot{N}_{visc} = -\frac{k \bar{p}}{\eta RT} \nabla p$$

The diffusive flux has the same form as in the free molecular flow regime but the diffusivity is an effective diffusivity. The effective diffusivity considers the effects of

Knudsen flow and traditional gas phase mass transport as given by Chapman-Enskog Theory [3-7] in series. The viscous diffusion term depends on the pressure gradient as well as the viscosity of the gas, η , the average pressure of the system, p , and the “apparent” permeability of the material, k .

In the continuum region, where $Kn < 0.01$, the contribution from viscous flow and diffusive flow are summed to determine the overall molar flux. However, in this region, molecular flow effects are very small and the diffusive term takes on traditional form with the diffusivity equal to the traditional gas-phase mass transport value as given by Chapman-Enskog Theory. Thus:

$$\dot{N} = \dot{N}_{vis} + \dot{N}_{diff}$$

$$\dot{N}_{diff} = -\frac{D_{12,gas}}{RT} \frac{\epsilon_p}{\tau_{p,Dif}} \nabla p$$

Scoping calculations for pressure driven diffusion using simple assumptions to understand the magnitude of some of the factors involved these have been performed. These equations have been used to estimate effective diffusivities as a function of pore or crack size. Kr gas at 1000° and 1600°C and pressures in the range of 0.5 MPa to 25 MPa, have been used to represent particle conditions representative of normal operation and accidents. Figure 3-7 then plots the effective diffusivities at 1000 and 1600°C respectively. The results suggest that gas pressure would only be important for characteristic sizes greater than ~ 0.02 microns. Furthermore, a comparison of the two figures suggests that the influence of temperature is moderate. The most important effect is that of the characteristic size of the transport path in the medium. For nanopores, effective diffusivities are on the order of 3 to $53 \times 10^{-7} \text{ m}^2/\text{s}$. By contrast, transport through micropores or micron sized cracks is much faster, with effective diffusivities ranging between 10^{-4} and $10^{-2} \text{ m}^2/\text{s}$ depending on the pressure of the gas involved. By way of comparison, the Germans assumed the diffusivity of all species in the buffer was $10^{-8} \text{ m}^2/\text{s}$ and the US used a value of $10^{-10} \text{ m}^2/\text{s}$ in their evaluations.

Although the actual pore size in the buffer is not well known, these results suggest that rapid transport of fission gases and fission product vapors could be expected through the buffer layer in a coated particle.

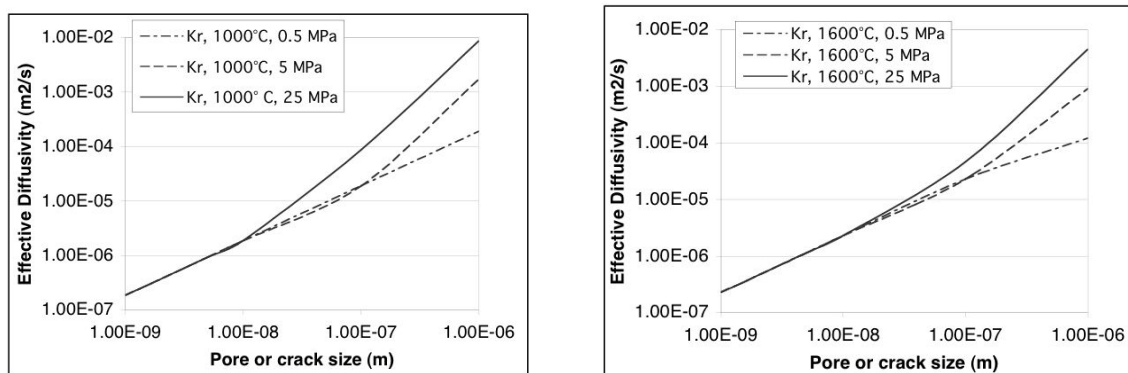


Figure 3-7 Calculated effective diffusivities for Knudsen and viscous diffusion

For these equations, the vapor species transport properties such as binary diffusion coefficients, viscosity and thermal conductivity would be needed for detailed analysis of fission product transport by gas phase mass transport. Very seldom are the properties of gaseous species measured. The transport properties of very high temperature gaseous species also have not been measured. These properties are typically calculated using formulae developed for example either by Chapman and Enskog or the formulae derived by Grad [3-9, 3-10]. In general, these formulae are not strictly applicable to the species of radiological importance because of assumptions related to the nature of collisions among the molecules. Calculations of collision integrals must consider inelastic collisions among the molecules. To do the collision calculations, it is necessary to have some information on the energy potential involved in the interactions of species such as a Lennard-Jones potential or a Sutherland potential. At the very high temperatures associated with coated particle fuel, one approach might be to assume that the vapor species all behave as hard spheres undergoing somewhat inelastic collisions.

For gas phase, mass transport scoping calculations, a formulation involving one gas and estimating the properties of the porous material may be utilized in the evaluation. Accurate modeling would require detailed information about the level of connected porosity and the tortuosity of the material (which can be determined by measurement) as well as an assumption about the nature of the porous material. Three common analytic models for porous materials are found in the literature for transport in graphite and catalysis.

In the parallel straight-channel model, the porous material is assumed to consist of parallel channels of diameter d_c . Then,

$$\frac{\varepsilon}{\tau} = E$$

$$K_0 = \frac{Ed_e}{4}$$

$$B_0 = \frac{Ed_e^2}{32}$$

For the parallel, tortuous channel model, [3-14] the model is the same as that above, except the channels are not straight:

$$B_0 = \frac{\varepsilon d_e^2}{40\tau}$$

$$K_0 = \frac{3\pi}{64} \frac{\varepsilon d_e}{\tau}$$

In the random channel or ‘dusty gas’ model, the porous solid is assumed to be composed of spherical grains of radius r_g with n_d grains per unit volume:

$$\frac{1}{K_0} = \frac{128}{9} \frac{n_d \tau}{\varepsilon} r_g^2 (1 + \pi/8)$$

The dusty gas and the tortuous channel models have been applied to graphite. In graphites, it is often found that there is a high degree of correlation between the Knudsen parameter and the Poiseuille parameter. Other models exist in the literature that account for the presence of distributions of voids and channel sizes in the porous materials. Within the catalysis literature, multiple populations of channels with distributions of sizes are considered. To use any of these models completely to calculate the molar flux, the porosity and tortuosity of the buffer need to be known or estimated. Such information has not historically been measured for HTGR fuel particles. Accordingly, the application of these models at this time to coated particle fuel would be limited to scoping calculations.

3.3.3. Thermal Diffusion

The large thermal gradients in the buffer discussed in Section 3.3, can lead to thermal diffusion, which must be added to the traditional concentration gradient driven Fickian diffusion across the layer. The combined diffusive flux for one species can then be written as:

$$J = -D(\nabla C + \frac{C}{RT^2} \nabla T)$$

where:

D = diffusion coefficient
Q* = heat of transport
T = temperature
J = diffusive flux
C = concentration

The second term on the right hand side of the equation is the thermal diffusion component, or Soret effect. Most of the literature dealing with thermal diffusion (the Soret effect) relates to gases or liquids. There are a few references dealing with solids. The heats of transport, Q*, for the buffer and condensable fission products combinations are unknown. However, the values of Q* range from about -210 kJ/mol to + 50 kJ/mol for various material combinations in the literature [3-15, 3-16, 3-17]. This corresponds to values of Q*/R from -25,000 K to + 6,000 K. A value of + 20,000 K can be considered to determine an upper bound for fission product transport through the buffer layer in the presence of a temperature gradient.

The influence of irradiation and thermal gradient on the release of fission products from an intact particle may be scoped out by modeling the kernel and each layer of the coated fuel particle using a one-dimensional diffusional transport code [3-18]. Based on the power per particle and the irradiation temperature, the temperature of each material constituent in the coated particle could be calculated. Based on the power level and time (burnup), the fission product generation can be calculated. Using the diffusivities of cesium in the kernel and layers in the TRISO coating from the German experience [3-5], a diffusivity of 10^{-7} m²/s in the buffer layer and a value of Q*/R of 20000 K, a calculation of the transport of fission products from the kernel and into the coatings under a specified irradiation history and a subsequent 500 hour isothermal heating at 1600°C may be used to simulate a traditional German accident heating test.

Figure 3-8 summarizes the result of these calculations. Plotted is the fraction of cesium in the OPyC layer at the end of the irradiation and the fraction of cesium released from the particle at both the end of irradiation and the end of the 500-hour high temperature heating for different particle powers. Two different irradiation conditions are considered: a three year constant irradiation at 1225°C and a 10-cycle 3-year pebble bed irradiation where the fuel experiences a change in temperature from 600 to 1200°C ten times over its three year life, as illustrated in Figure 3-4.

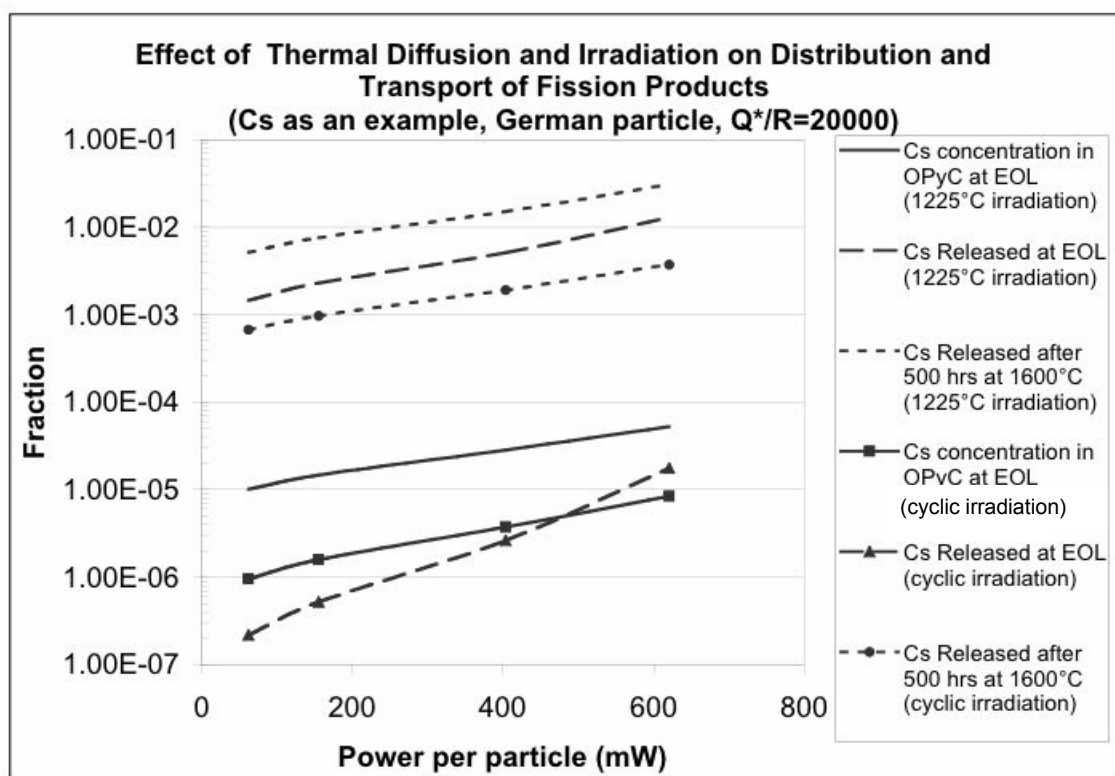


Figure 3-8 Calculated effect of thermal diffusion and irradiation on the distribution and transport of fission products in the coated particle

The calculated results would indicate that the cyclic irradiation has a strong influence on the distribution and transport of fission product cesium. The analysis indicates an order of magnitude more cesium reaching the OPyC layer in the case of the 3-year constant irradiation at 1225°C than in the case of cyclic irradiation, and three to four orders of magnitude more cesium released from the particle at the end of irradiation in the case of constant irradiation at 1225°C than in the case of cyclic irradiation. After the 500-hour high temperature heating, the cesium release from the particle is an order of magnitude greater in the case of constant irradiation at 1225°C than in the case of cyclic irradiation. These results would indicate that the irradiation history has an effect on the concentration of fission products in the layer and the subsequent release from the particle.

The analytical results also indicate that thermal diffusion (Soret effect) can have a moderate influence on the transport and distribution of fission products. A factor of ten increase in power per particle (from 60 mW to 600 mW) would increase the concentration of cesium in the OPyC and the fraction of cesium released after irradiation and after high temperature heating by factors of 5 to 10.

These results indicate the important role of irradiation history on both the distribution of fission products in the coated particle and their release under normal operation and potential accident conditions. Irradiation has a large impact on the fission product

behavior in the accident because of the effects of the initial distribution of fission products in the particle. However, for low power/thermal gradients in German pebbles (and the low level of acceleration in most German irradiations [3-19]), thermal diffusion would be expected to be much less important in (modeling of) fission product release. In cases where the irradiations are of very high power (such as the very accelerated US fuel irradiations that have occurred in U.S. fuel irradiates in the past) thermal diffusion would be expected to be important. However, when the full multicomponent nature of the problem and the effects of pressure diffusion and thermal diffusion are considered together, the results may show a greater effect of thermal diffusion than the simpler calculations presented here.

3.4 The Inner and Outer Pyrocarbon Layers

The inner and outer pyrocarbon layers are dense layered carbon structures. The goal during fabrication is to make the pyrocarbon as isotropic as possible during the deposition to ensure the best radiation stability of the layer, which is needed for particle integrity.

Some data exist on effective diffusivities in the PyC layers. Measured values from BISO particles (without SiC) have been collected and the results shown in Figure 3-9. [5] These data suggest that a dense, intact pyrocarbon layer is a very good barrier to noble gas release with significant diffusional releases not observed until temperatures near 2000°C are reached. The PyC layers do not provide significant barriers to release of cesium, silver and strontium metallic fission products under normal or accident conditions.

The mechanism responsible for the transport of gaseous and metallic fission products in the PyC layer has not been the subject of significant worldwide study. An understanding of the mechanism responsible for noble gas transport in PyC is limited. A comparison of different measurements and calculations are overlaid on the original diffusivity data in Figure 3-10.

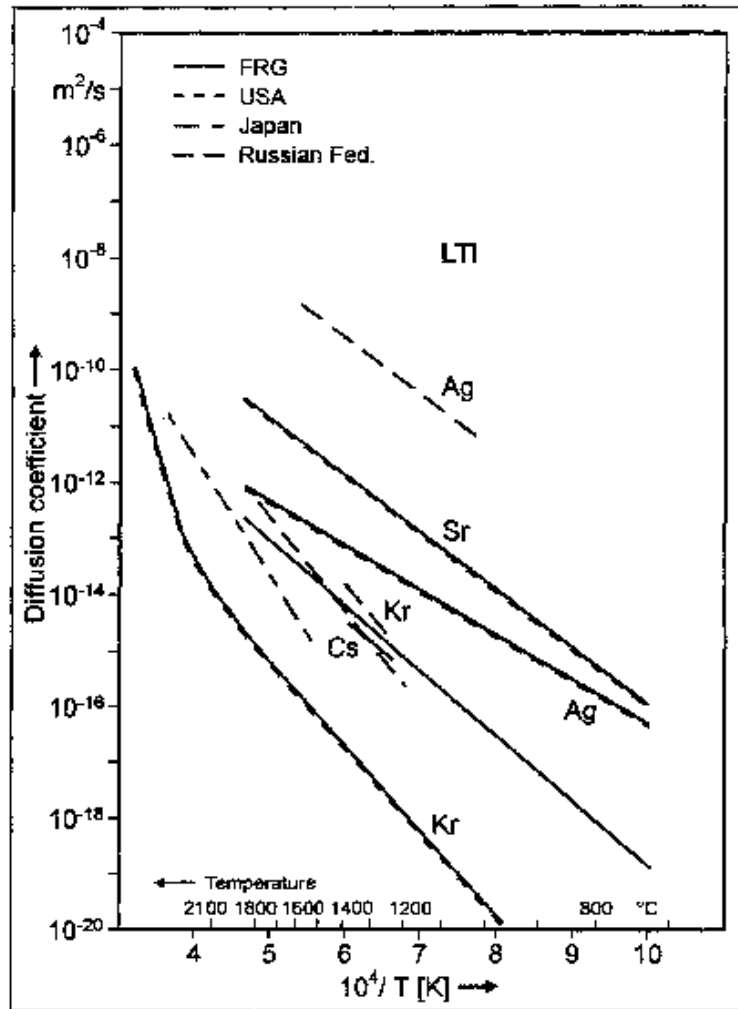


Figure 3-9 Measured fission product diffusivities in low temperature isotopic (LTI) PyC

3.4.1. Gas Phase Fission Product Transport

The measured diffusion coefficients suggest very slow transport through the inner PyC layer. Permeability measurements using He and CO [3-20] indicated in Figure 3-10, suggest very slow transport of these gases consistent with the measured fission product diffusivity. By contrast, diffusion predicted by the Knudsen diffusion model in Section 3.2.3 for nano-porosity or viscous diffusion for micro-porosity if applied to the PyC layer would predict transport rates that are 6 to 10 orders of magnitude faster than the measured data on BISO particles. These results may suggest either (a) Knudsen diffusion of noble gases is extremely small in PyC perhaps because the interconnected porosity is very low or (b) that Knudsen diffusion is not the mechanism responsible for noble gas transport in PyC.

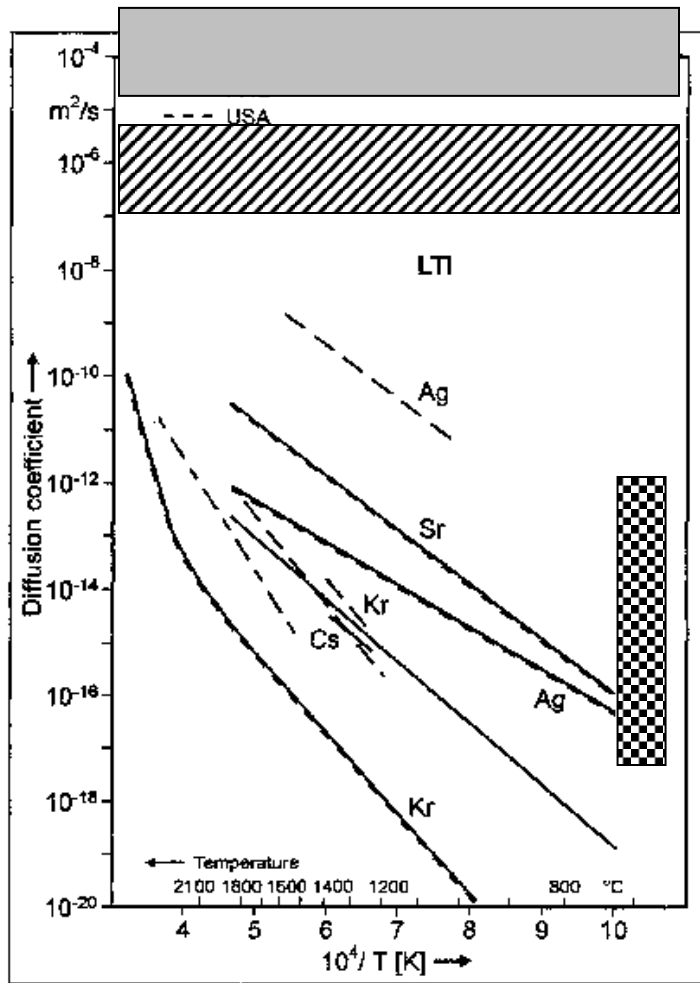


Figure 3-10 Comparison of measured fission product diffusivities in PyC to permeability data, (checkerboard box) Knudsen data, (black and white hatched box) and viscous (gray box) diffusion estimates

3.4.2. Metallic Fission Product Transport and Trapping

For some of the fission metals like cesium and strontium and even iodine, [3-21, 3-22, 3-23, 3-24] transport behavior in intercalated graphite may be important. Intercalation, the insertion of guest atoms into a host structure, has been studied extensively and a diffusion and trapping mechanism has been proposed as the mechanism responsible for the resultant transport behavior in the material [3-25]. Thus, intercalation may be the mechanism responsible for the transport of Cs, Sr and perhaps even iodine and CO in the PyC. A classic diffusion and trapping model has been proposed for modeling the transport, with trapping occurring perhaps at the carbon crystallite edges and defects in the graphitic material. (Trapping is the capture of atoms at the atomic level by physical defects or chemical interaction that impedes transport.)

Diffusion and trapping can be modeled using a simple modification to classical Fickian diffusion as shown in the following equations. [3-18]

$$\begin{aligned}\frac{\partial C}{\partial t} &= D \nabla^2 C - \frac{\partial C_T}{\partial t} \\ \frac{\partial C_T}{\partial t} &= w \frac{x_T}{N} C - r C_T \\ x_T &= x_T^0 - C_T\end{aligned}$$

Trapping impedes diffusion. Many times a concentration dependence of diffusivity is observed, which is an indication that trapping is involved. As the traps get filled at high atom concentrations in the material, the observed transport increases. Thus, one can also write an expression for an apparent diffusivity as follows [3-26]:

$$D_{app} = \frac{D}{(1 + \frac{wx_T}{rN})} = \frac{D}{(1 + \frac{D_o}{\lambda^2 \nu_o} \exp(\frac{E_{trap} - E_{diff}}{kT}) \frac{x_T}{N})}$$

Where:

- D_{app} = apparent diffusivity (m²/s)
- D_o = pre-exponential of diffusivity (m²/s)
- D = diffusivity (m²/s)
- w = trapping rate(/s)
- r = resolution or release rate from the trap(/s)
- λ = jump distance (m)
- ν_o = Debye frequency (/s)
- X_T = empty trap density (atoms/m³)
- E_{trap} = trap energy (ev)
- E_{diff} = diffusion constant activation energy (ev)
- N = number density of host material (atoms/m³)

An initial concentration of empty traps is assumed to exist in the material and a mass balance on the traps is performed to determine when all of the trapping sites are occupied. To model the behavior in detail, the trap concentration or trap density is required as well as the energy of the trap, which is important to model release from the traps accurately. Irradiation is known to result in the production of traps via defect formation and thus can increase the complexity of the analysis model.

A few simple parametric and sensitivity calculations can be used to understand the magnitude and importance of trapping in PyC layers of TRISO-coated particle fuel. Figure 3-11 plots the diffusion coefficient of Cs in PyC⁴ and SiC along with the apparent Cs diffusion coefficient in PyC for different trap concentration levels from 10 to 5000 ppm using the measured 4 ev trap energy for graphite.

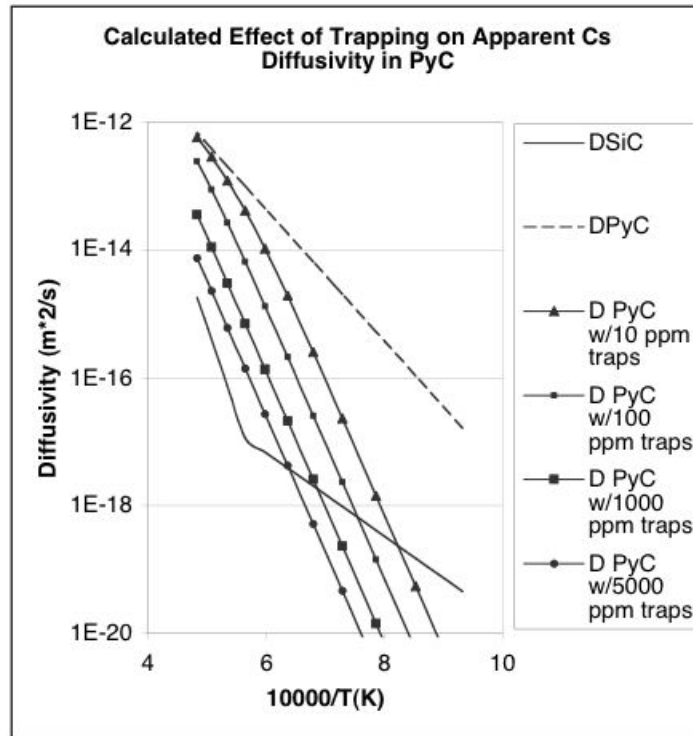


Figure 3-11 Calculated effects of trapping on apparent Cs diffusivity in PyC

The transport through the TRISO coating will then be controlled by the lowest diffusivity in the figure. Under accident conditions, the SiC diffusivity is the lowest suggesting it is the greatest barrier to cesium release. Under normal operating temperature (800-1200°C), trapping can lower the apparent diffusion coefficient in PyC significantly. A comparison of the apparent diffusivities in the PyC with that of PyC with no traps suggests that the apparent diffusion coefficient can be four to five orders of magnitude lower than the intrinsic diffusivity depending on the trap concentration. At the higher temperatures, the release rate from the traps is so large that the effects of trapping is diminished somewhat.

Diffusion and trapping are dynamic factors. As atoms diffuse through the layer, a certain fraction is trapped. As these traps are filled, the apparent diffusivity increases. The

⁴ Existing German data were measured on BISO particles. Concentrations are probably high enough that trapping effects were small and thus the measured diffusion coefficients are representative of transport without trapping.

magnitude of the intrinsic diffusion coefficient in PyC (i.e., without traps is high enough that significant diffusion of cesium into the PyC is expected during normal operation. The Cs concentration in IPyC is expected to be much greater than the trap density, perhaps at the level of 0.5 to 1% atom concentration, so the traps would fill quickly and not in and of itself affect overall transport behavior. In a heat-up event, in which SiC layer might fail, release of Cs inventory from the IPC layer will not be influenced significantly by trapping. Thus, it may be concluded that trapping is not an important effect in the transport behavior in the IPyC layer. However, in the OPyC layer, the Cs concentration in OPyC is much smaller, on the order of the trap concentration expected in graphite. Thus, in the OPyC layer the traps can effectively compete for these Cs atoms, which could result in a much slower transport.

Similar analysis for Sr suggests that given the very low release of Sr from the kernel during operation, the Sr concentration in the IPyC would be at the high end of the trap concentration and thus may not be influenced by trapping. In the OPyC, the Sr concentration is much smaller and trapping effects could be very important.

3.4.3. Influence of PyC Structure on Transport in the Layer

Pyrocarbon has a complex structure made up of different “growth features”, the shapes of which can vary depending on the deposition conditions, specifically coating temperature and coating gas composition. Three different types of growth features have been observed: (a) a three dimensional mosaic of tightly packed crystallites with little porosity between the crystallites, (b) small crystallites arranged in the form of long twisted ribbon or fibers which contains a considerable amount of porosity and (c) large crystallites that are layered. Fission product transport at the microscopic level in this layer (intercalation and trapping at the edge of the crystallites for example) depends on the nature of these three types of growth features. A complete understanding of the relationship between structure and transport is lacking. The differences in measured effective diffusion coefficients in the U.S., Germany, Russia and Japan, as shown in Figure 3-9 may reflect differences in the structure of the PyC which may be related to differences in the relative amounts of the different growth features because of differences in PyC coating conditions. Thus, for manufactured TRISO fuel, it is important to establish that the transport-structure relationship implicit in the data in Figure 3-9 is also valid for the newly produced fuel, if the PyC diffusivities shown in the figure are to be used in a fission product transport analysis. This might be accomplished by (a) demonstrating that the PyC produced in the new fuel was fabricated under coating conditions that are the same as that used in the past and has similar structure to that in the literature, and (b) demonstrating by experiment that fission product transport is similar to that measured previously by others. Significant deviations from the historic transport-structure relationship could indicate that the historic experimental database on fission product transport for TRISO-coated particle fuel might not be applicable to the new fuel that is produced.

3.5 The SiC Layer

SiC in TRISO-coated particle, fuel is a high-density polycrystalline beta-SiC. It is the major fission product barrier in the fuel. As with the pyrocarbon layers, data on the effective diffusion coefficients of noble gases, cesium, strontium and silver have been inferred from integral release measurements [3-5]. Figure 3-12 plots the effective diffusion coefficient for noble gases, cesium, strontium and silver.

3.5.1. Transport Mechanisms

The mechanisms responsible for the transport of gaseous and metallic fission products in the SiC layer have not been the subject of significant study worldwide. An understanding of the mechanism(s) responsible for fission product transport in SiC is limited. A Knudsen diffusion mechanism could be postulated for the transport of noble gases and Ag vapor through the SiC layer especially under normal operating conditions. The interconnected porosity of the SiC layer is expected to be quite small because the beta-SiC is very high density (3.21 to 3.23 g/cc is commonly fabricated). Research is being conducted to understand Ag transport through SiC [3-27]. Under accident conditions, bulk diffusion may play an increasing role in the transport.

For the other metallic fission products, a mixture of grain boundary and bulk diffusion has been postulated depending on temperature, with grain boundary diffusion most likely at low temperatures (e.g., <1000°C) and bulk diffusion at high temperatures (e.g., 1400-1800°C) representative of accidents. The magnitudes of the activation energies in Figure 3-12 tend to support this theory. A comparison of the effective diffusion coefficients for fission gases, Cs, Sr and Ag in SiC with more recent measurements on other species in SiC can be used to infer the potential underlying mechanisms. Figure 3-13 overlays the original data with self-diffusion data for C and Si in SiC (hatched box) and grain boundary diffusivities for Fe, Cr (gray box) [3-28, 3-29]. The magnitude and slopes of the grain boundary diffusivities for Fe and Cr are similar to that for Cs and Sr perhaps suggesting that grain boundary diffusion may be the dominant mechanisms for Cs and Sr transport through SiC. The slope of the C and Si diffusion coefficients are similar to that for Xe at high temperature suggesting that a vacancy mechanism may describe noble gas transport in SiC.

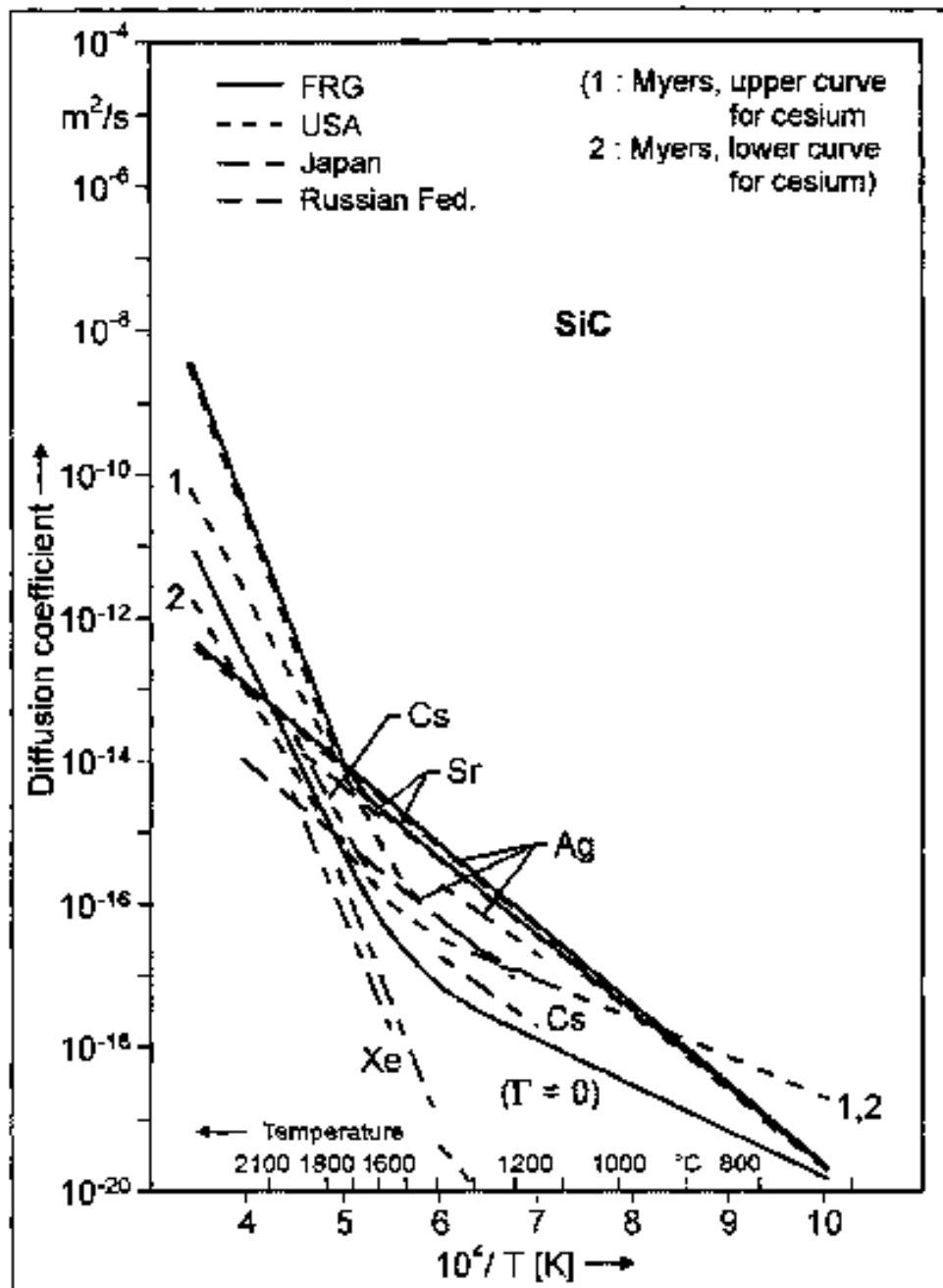


Figure 3-12 Measured diffusion coefficients of Xe, Cs, Sr and Ag in SiC

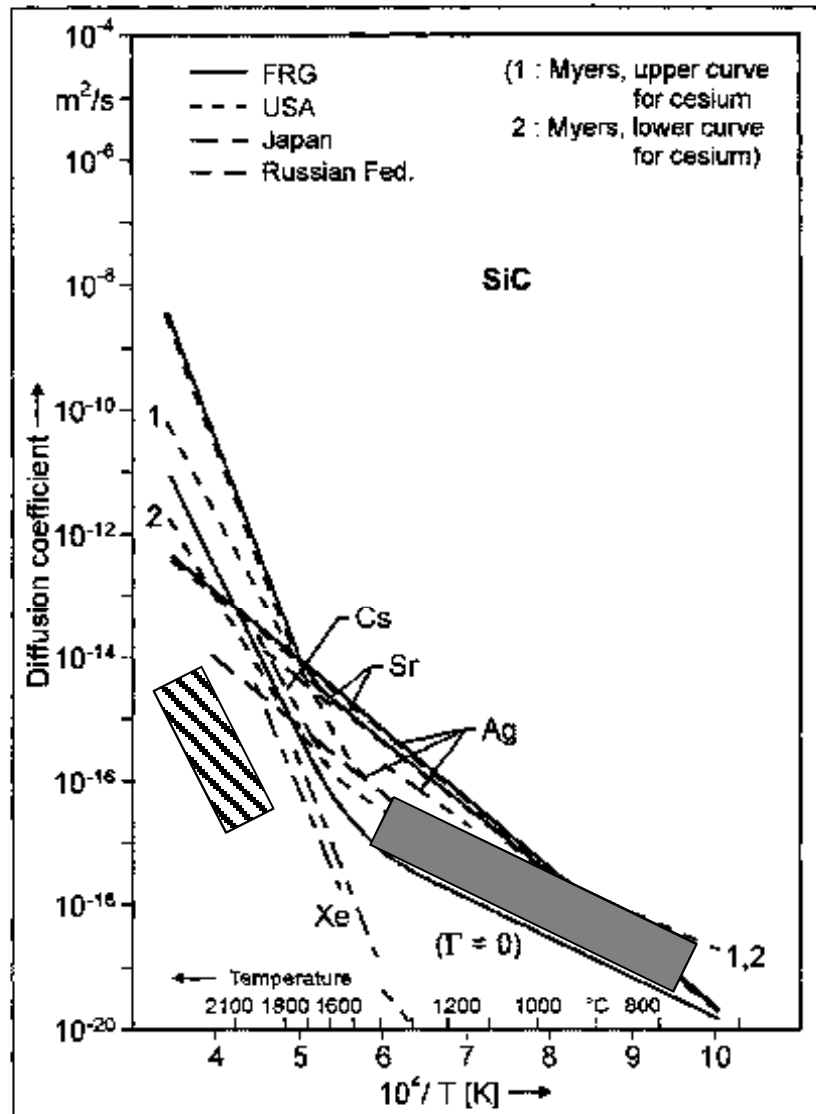


Figure 3-13 Comparison of data for C and Si self-diffusion coefficient (hatched box) and Fe and Cr grain boundary diffusivities (gray box) with fission product diffusivities inferred from integral release measurements on coated particles

3.5.2. Grain Boundary Diffusion

Grain boundary and bulk diffusion may be important in describing fission product transport in coated particle fuel. The importance of each mechanism depends on the temperature, the individual diffusivities in the bulk and along the grain boundaries, and the area fraction occupied by grains and boundaries. Grain boundary diffusion has been studied extensively. It can act as a fast diffusion channel in polycrystalline materials.

Fast diffusion sometimes manifests itself as a very high pre-exponential factor, D_0 , in the measured diffusion coefficients. The classic Arrhenius formalism suggests that D_0 should be on the order of the product of the Debye frequency and the square of the lattice spacing for atomic diffusion. (For many materials this is $\sim 10^{-3} \text{ m}^2/\text{s}$). However, experimental values can be 10^7 greater than this value [3-30] and may be related to the presence of grain boundaries, defects and surface effects. The influence of grain boundaries has been studied extensively and three different kinetic regimes have been found: Type A, B and C [3-31]. Figure 3-14 sets up the analytic picture of a grain boundary of thickness, δ . The grains are of width d and a uniform concentration of the fission product, C_0 , exists across the grains and grain boundary. A segregation coefficient, s , describes the ratio of the concentration in the grain and in the boundary at the surface interface. Solutions are then sought to the classic Fickian diffusion equations in two dimensions in both the grain, denoted by subscript v in the figure, and the grain boundary, denoted by subscript gb , in the figure.

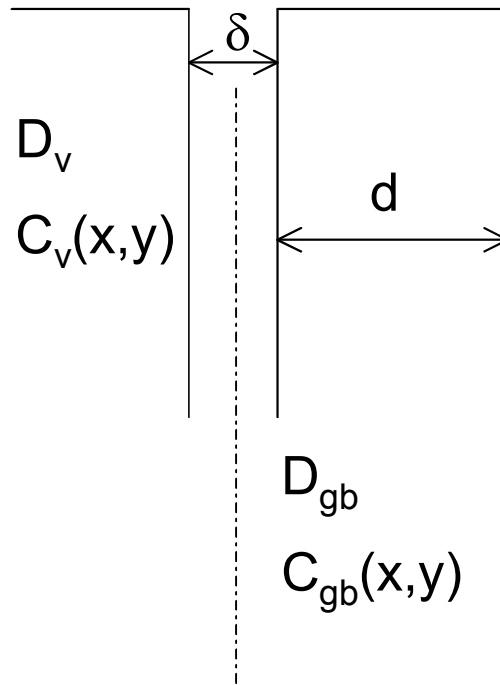


Figure 3-14 Schematic of grains and grain boundary

In Type A grain boundary diffusion, the penetration distance into the grain is much greater than the grain boundary thickness. In this case, both grain boundary and bulk diffusion are operative as would be the case for high temperatures and long heating times as is the case in safety testing of fuel particles. In this case, an effective diffusion coefficient is measured which is a volume weighted average of the bulk and grain boundary diffusion coefficient. The concentration profile is given by a classic complementary error function using the effective diffusivity. For Type A kinetics, these conditions are summarized below.

$$(D_v t)^{1/2} \gg d$$

$$c_b = s c_v$$

$$D_{eff} = f D_v + (1 - f) D_{gb}$$

$$\bar{c} = \text{erfc}\left(\frac{y}{2\sqrt{D_{eff}t}}\right)$$

In Type B kinetics, there is much greater penetration along the boundary than into the grains. In this case, what is actually measured is an apparent diffusion coefficient sometimes denoted as P_{gb} , which is the product ($s \delta D_{gb}$). This regime may be applicable at high irradiation temperatures. The analytic conditions for Type B kinetics and the resultant solution to the diffusion equations are given by:

$$s\delta \ll (D_v t)^{1/2} \ll d$$

$$P_{gb} = s\delta D_{gb} = 1.322 \sqrt{\frac{D}{t}} \left(-\frac{\partial \ln \bar{c}}{\partial z^{6/5}}\right)^{-5/3}$$

where the partial derivative term is the measured concentration profile in the sample.

In Type C kinetics, bulk diffusion is “frozen out” and the transport is dominated by grain boundary diffusion [$(D_v t)^{1/2} \ll s\delta$]. This is probably applicable at very low temperatures, conditions that may be representative of average irradiation temperature experiments. In this case, the concentration is given by a Gaussian for a point source and an error function for constant source with the effective diffusivity equal to the grain boundary diffusivity, D_{gb} .

These idealized situations are useful to understand the concepts of grain boundary and bulk diffusion in polycrystalline material. However, in practice the microstructure of the material is more complex. The application of mixed grain boundary and bulk diffusion in SiC would require development of appropriate mixture rules to establish an effective diffusivity through the structure. This is an area of active research [3-32]. Figure 3-15 compares three different idealized microstructures that may bound that expected in SiC as oriented relative to the SiC layer thickness. The large radially oriented columnar structure, which is found in some SiC, is idealized in the left portion of the figure. In this idealized case, the volume weighted mixture rule for the effective diffusivity would appear to be appropriate. At the other extreme is the case of SiC with an idealized circumferentially oriented laminar structure. In this case, a reciprocal series approach to establishing the effective diffusivity may be appropriate. In the middle of the figure is an idealized schematic representation of small-grained SiC, which is the form most sought

after in coated particle fuel. In this case, there is no exact mixture rule to use, but the two extreme cases would appear to bound the actual behavior.

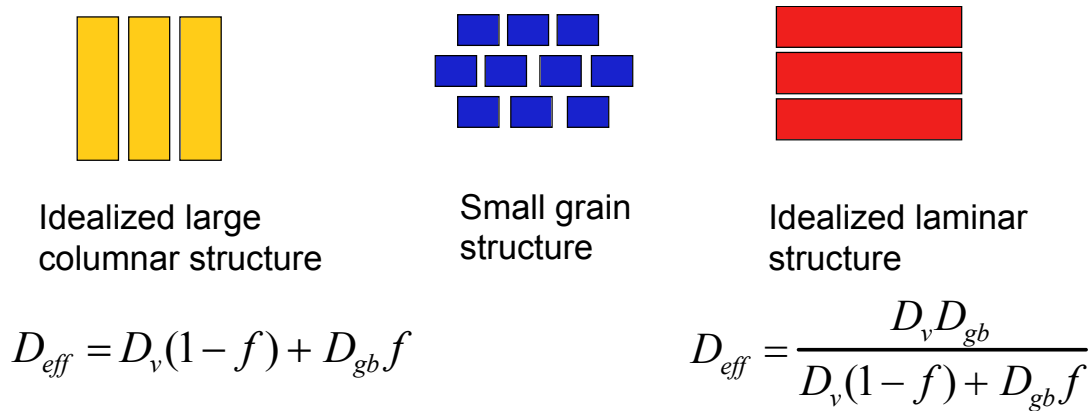


Figure 3-15 Influence of microstructure on apparent diffusivity

3.5.3. Influence of SiC Microstructure on Fission Product Transport

The previous section presented the concept that fission product transport in the SiC in temperature range of interest could be a mixture of bulk and grain boundary diffusion. Grain boundary diffusion is very sensitive to the microstructure of the material (e.g., grain size, fraction of the area occupied by grain boundaries, width of grain boundaries, segregation effects at the grain/grain boundary interface) and as noted earlier large differences in diffusivities have been noted in the literature and attributed to characteristics of the microstructure as well as defects and surface effects. Furthermore, there are little data on individual diffusivities of the important fission products in both single crystals and in polycrystalline material that are needed in these models. In the absence of such data, SiC effective diffusivities have been utilized and have been inferred from fuel element integral release measurements.

There is also a limited understanding of the linkage between transport, microstructure and deposition conditions for SiC. Although most historical work on SiC has focused on optimizing deposition conditions to produce small-grained SiC, the literature is full of examples where changes in deposition conditions, especially coating temperature, can result in large, radial, columnar structures at higher temperatures and laminar structures at lower temperature. At coating temperatures below 1450°C, some alpha-SiC and/or excess silicon is obtained. The structure is striated with no evidence of individual grains. Smaller, fine-grained SiC is obtained using a coating temperature between 1500 and 1550°C. Above 1600°C, large, radial, columnar grains of SiC are obtained, with the crystallite size increasing with increasing temperature. [3-33, 3-34, 3-35] These results suggest that as in the case of pyrocarbon, any new fuel that is produced which would seek to reference the transport behavior shown in Figure 3-12 would have to establish that the transport-structure relationship implicit in the data in Figure 3-12 is also valid for the newly produced fuel. This might be accomplished by (a) demonstrating that the SiC

produced in the new fuel was fabricated under coating conditions that are the same as that used in the past and has similar microstructure (e.g., small grained SiC), and (b) demonstrating by experiment that fission product transport is similar to that measured previously by others. Significant deviations from the historic transport-structure relationship indicate that the historic experimental database on fission product transport for TRISO-coated particle fuel might not be applicable to the new fuel that is produced.

3.6 A Simplified Integral Fission Product Transport Model

In the previous sections, the transport mechanisms in each layer have been reviewed. In this section, a simplified integral model is developed for release from TRISO-coated particle fuel using some of the ideas and data in the previous sections. Some preliminary calculations using the model are also presented.

Morgan and Malinauskas [3-36] developed an analytic solution for depletion of a fission product through a single coating layer given by:

$$FR = 1 - \frac{Ka}{b} \sum_{n=1}^{\infty} \frac{\exp(-D^* t \alpha_n^2 / \delta^2) \sin(\alpha_n)}{[2K\alpha_n + (4b\alpha_n / \delta) \sin^2 \alpha_n] + K \sin(2\alpha_n)}$$

where

$$\cot(\alpha_n) = (b\alpha_n / K\delta) - (\delta / b\alpha_n)$$

$$K = (A/V)s$$

a = the inner radius of the coating,

b = the outer radius of the coating,

A = the surface area of the inside of the coating,

V = the volume inside the coating, and

S = segregation factor (ratio of surface layer concentration to source concentration).

If the TRISO coating is considered a composite layer then the simple resistance concept to model can be used for all three layers as one layer and write the apparent diffusivity D^* as

$$\frac{\delta}{D^*} = \frac{\delta_{IPyC}}{D_{IPyC}^{eff}} + \frac{\delta_{SiC}}{D_{SiC}^{eff}} + \frac{\delta_{OPyC}}{D_{OPyC}^{eff}}$$

Where δ is the total thickness of the three high density TRISO coatings.

This simple model uses effective diffusivities for each layer and can account for trapping if needed, transport through cracks or pores, and different microstructures. The model also accounts for the effects of a depleting source and can consider partitioning(s) between coating layer and kernel.

This model can be used in conjunction with the Booth release model from the kernel to calculate the diffusional releases from the particle during a constant 1600°C heating and a depressurized conduction cool down. Thermal diffusion is not included in the model and no segregation was assumed ($S=1$). (Note that the matrix material sorbs metallic fission products and thus the results are not a complete model for the entire fuel element. As referenced earlier, the model should be viewed as a scoping tool to understand what factors and factors are important to fission product transport in the particle.)

Figure 3-16 and Figure 3-17 plot the calculated fractional release for various fission products during post irradiation heating at 1600°C following a constant three year irradiation at 1200°C typical of a peak fuel particle in a prismatic gas reactor and a ten cycle three-year 600 to 1200°C cyclic irradiation expected in a pebble bed reactor. The results suggest that the irradiation temperature has at best a modest influence on the release at high temperature, given the long time at temperature in these calculations.

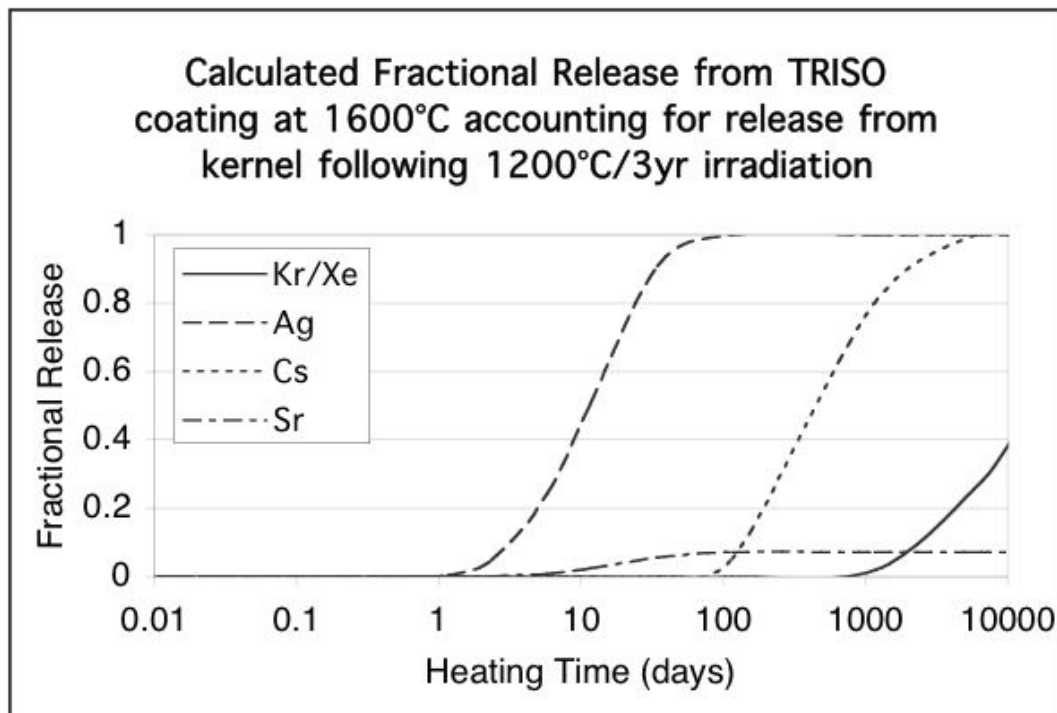


Figure 3-16 Calculated fractional release from a coated fuel particle during 1600°C heating following a three year irradiation at 1200°C

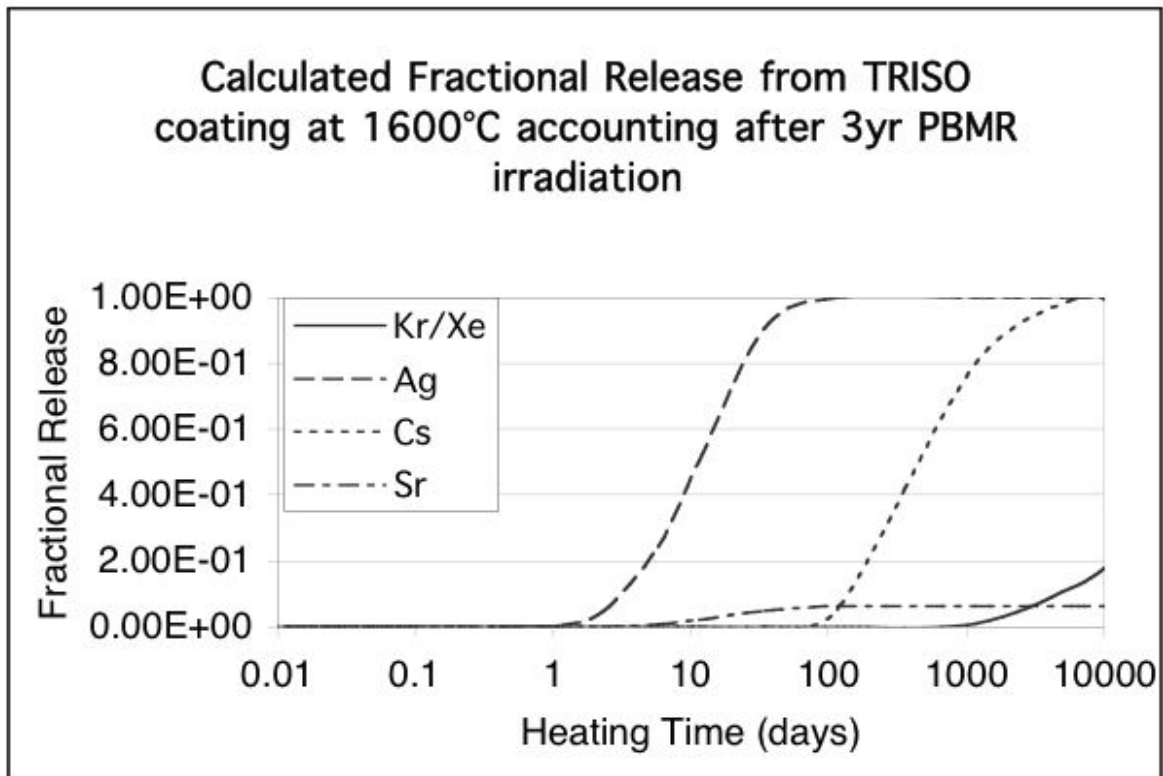


Figure 3-17 Calculated release from a coated fuel particle during 1600°C heating following a three-year ten-cycle PBR irradiation between 600 and 1200°C

The calculated diffusional releases from a conduction cool down (see Figure 3-18) following a PBR irradiation are shown in Figure 3-19. The conduction cool down is characterized by a slow heatup in the maximum fuel element temperature to a peak temperature of ~ 1600°C followed by a gradual temperature decline over the course of hundreds of hours.

By comparison to the releases during a constant high temperature heating in Figures 3-16 and 3-17, only silver and strontium releases from the particle are calculated given the magnitude of the diffusivities in the layers and the time/temperature profile in the accident scenario given in Figure 3-18. These results illustrate the importance of time at temperature on the magnitude and time of the calculated releases.

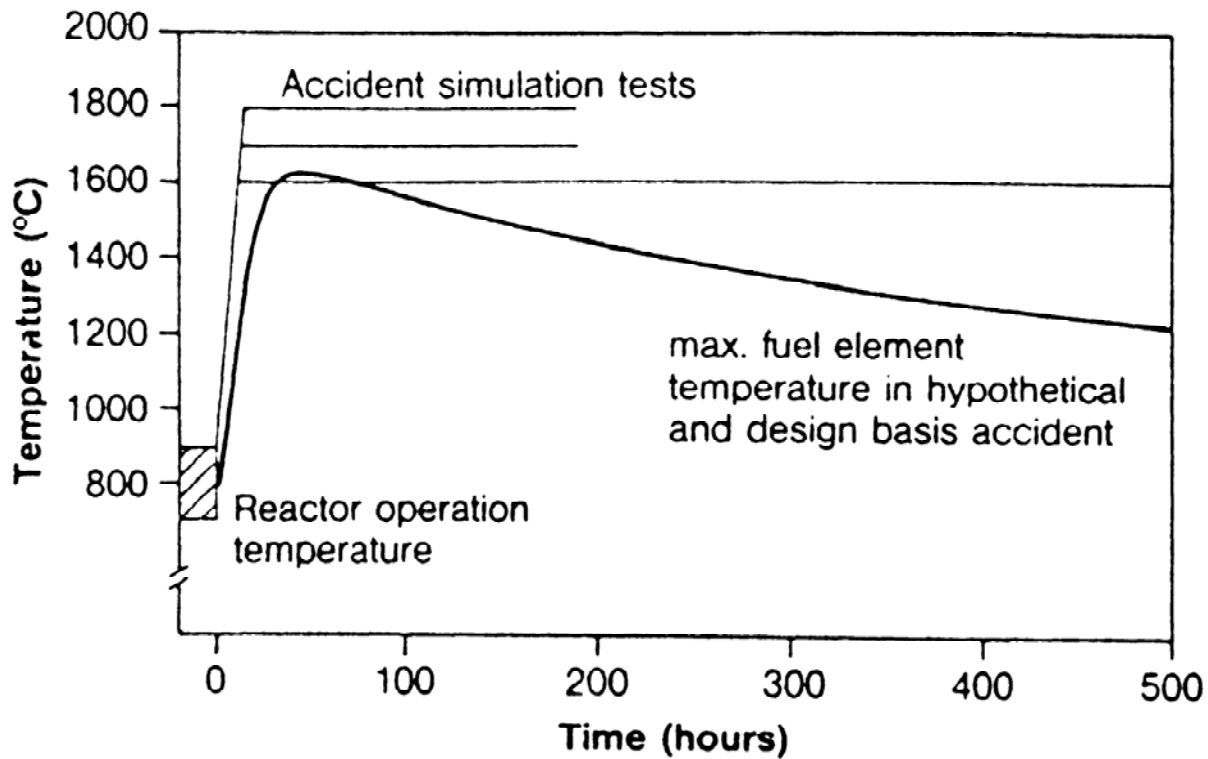


Figure 3-18 Calculated fuel temperature transient during a conduction cooldown

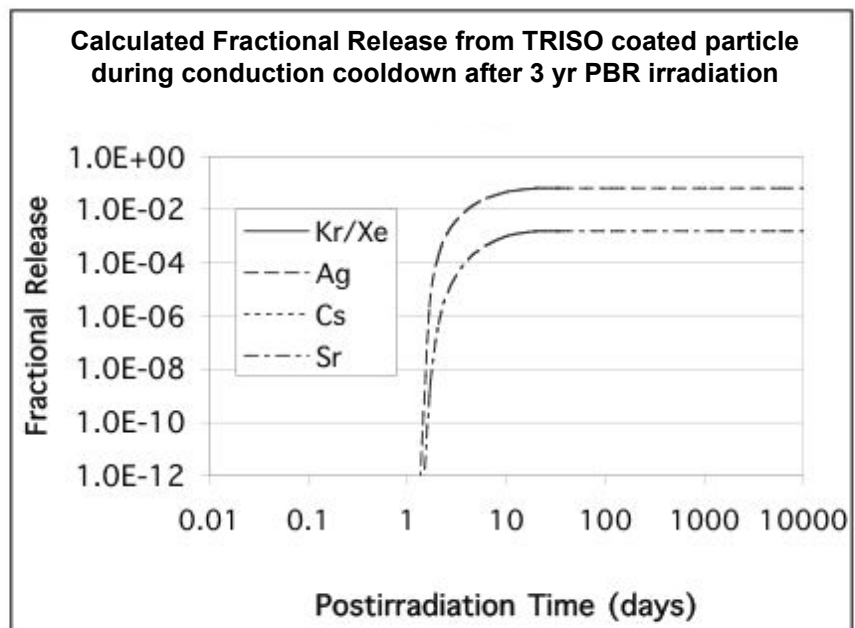


Figure 3-19 Calculated fractional diffusional release from TRISO coated particle during a conduction cooldown following a three-year ten-cycle PBR irradiation

Table 3-3 presents the results of two sensitivity studies: (a) a case where all temperatures are increased by 100°C and a case where the diffusivity in the SiC layer has been increased by a factor of 10 over the base value. The results show a modest impact of between two and six on the overall release for silver and strontium and little impact on either noble gases or cesium.

Table 3-3. Calculated Effect of Increased Temperature and Increased SiC Diffusivity on Fractional Diffusional Releases from TRISO Coated Particles.

Fission Product	Case		
	Base	+100 °C	10X SiC Diff
Kr/Xe	0	0	0
Ag	0.27	0.59	0.98
Cs	0	0	2.54E-05
Sr	0.0098	0.026	0.06

As a final sensitivity study, the influence of the segregation factor on the overall diffusional release from the particle was examined. The segregation factor coefficient can be used to account for the build up of fission products that may occur near cracks because of the fast diffusion at the grain boundary. Figure 3-20 plots the fractional release versus dimensionless time for four different segregation coefficients (1, 5, 10, 50).

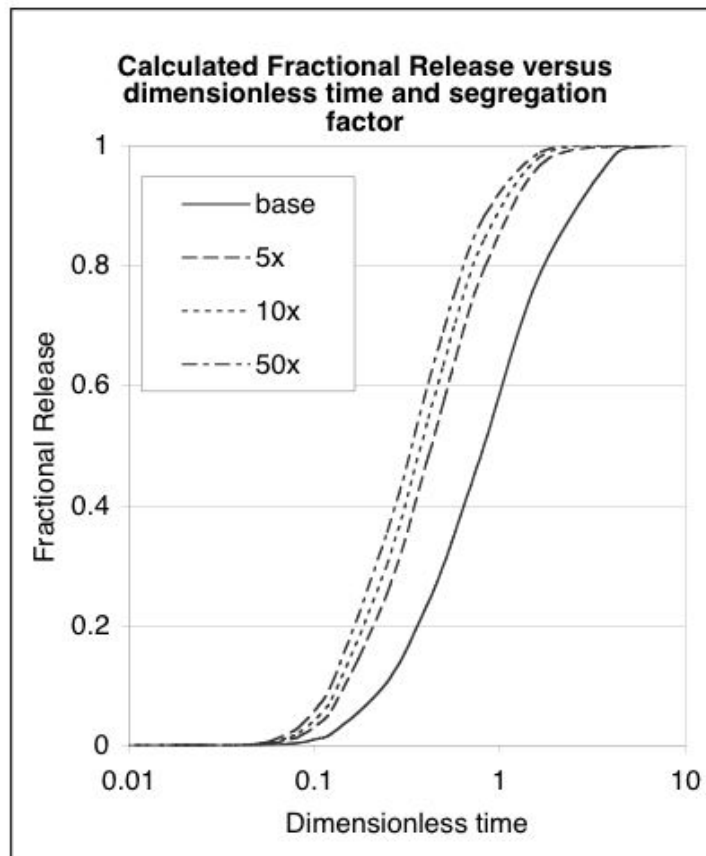


Figure 3-20 Effect of segregation coefficient on fractional release during heating

The results suggest that the fractional release of a fission product at a given time can differ by a factor of two to three depending on the magnitude of the partitioning that exists at the interface. Reference [3-5] suggests that segregation factors between 0.3 and 3 have been measured for some fission products. The simple calculation suggests that segregation or the build up of fission products at the interface between layers may explain some of the variability that has been observed in heating tests of coated particles irradiated to nominally the same conditions. The model presented here, although simple, can help scope out the importance of different reactor parameters on the source term from an ATGR.

3.7 Fission Product Transport in Failed Fuel Particles

Fission product transport in failed fuel particles is expected to be a major contributor to the gas reactor source term. Fission product release from uranium contamination in the fuel element matrix (compact or sphere) as well as from particles with missing layers may also be significant contributors. The transport model depends on the half-life of the fission product and whether it is metallic or gaseous.

3.7.1 Short-lived Fission Gases. For short-lived fission gases, the release is expressed in terms of the release rate to the birth rate (R/B) ratio for the particular fission gas. The R/B is from failed particles and from uranium contamination in the fuel element matrix (compact or sphere) is expressed for gas specie i as:

$$(R/B)_i = f_{\text{fail}} (R/B)_{\text{fail},i} + f_{\text{U-contamination}} (R/B)_{\text{U-contamination},i}$$

where

f_{fail} = particle failure fraction

$(R/B)_{\text{fail},i}$ = release rate to birth rate ratio per particle failure for gas specie i

$f_{\text{U-contamination}}$ = uranium contamination fraction

$(R/B)_{\text{U-contamination},i}$ = release to birth rate for gas specie i due to U contamination.

The uranium contamination is based on the elemental impurity level in the compact matrix material as determined by chemical methods. The sum of the heavy metal contamination and the initial failed particle level is determined by QC measurements on the fuel elements via destructive burn leach measurements. Subtraction of the burn leach results from the chemical results on the fuel element matrix material will provide the initial particle failure fraction. (Subsequent failures under irradiation would add to this source term.) The (R/B) correlations are based upon the Booth equivalent sphere gas release model. These correlations may be generally expressed as [3-37]:

$$(R/B) = (3/x) [\coth(x) - (1/x)]$$

where

$$x = [(\lambda a^2) / D]^{1/2}$$

$$\lambda = \text{decay constant for the fission gas isotope} = \ln 2 / T_{1/2} \text{ (s}^{-1}\text{)}$$

$$T_{1/2} = \text{isotope half life (s)}$$

$$D/a^2 = D' = \text{reduced diffusion coefficient (s}^{-1}\text{)}$$

$$a = \text{radius of equivalent sphere (m)}$$

$$\coth(x) = [\exp(x) + \exp(-x)] / [\exp(x) - \exp(-x)].$$

The equivalent sphere radius, a, is equal to the kernel radius when considering (R/B) for failed particles and is proportional to the raw graphite grain size of the matrix when considering (R/B) from uranium contamination.

Several correlations for reduced diffusion coefficients to be used in (R/B) calculations exist in the literature [3-5]. A few of the frequently referenced correlations are:

The US Model [3-38] which contains a unique reduced diffusion coefficient correlation and also differs from the classic Booth Equivalent Sphere formalism presented above in that it contains a diffusion parameter, multiplicative temperature and burnup functions and an empirical factor.

The British Model [3-2] that incorporates intrinsic diffusion, vacancy diffusion and athermal diffusion (a function of fission rate density) terms in its reduced diffusion coefficient.

The German I and II Models [3-39] that incorporate two separate sets of temperature-dependent reduced diffusion coefficients.

A comparison of the four models for Kr-85m (R/B) per failed particle is presented in Figure 3-21. Input parameters for this comparative calculation are representative of fuel irradiated in the NPR-1A experiment. On-line gas release measurements from the experiment indicated that Kr-85m (R/B) per failed particle was 0.028 at a time-average volume-average temperature of 977 °C. [3-40]. This experimental value compares almost exactly with the calculated German II value of 0.029.

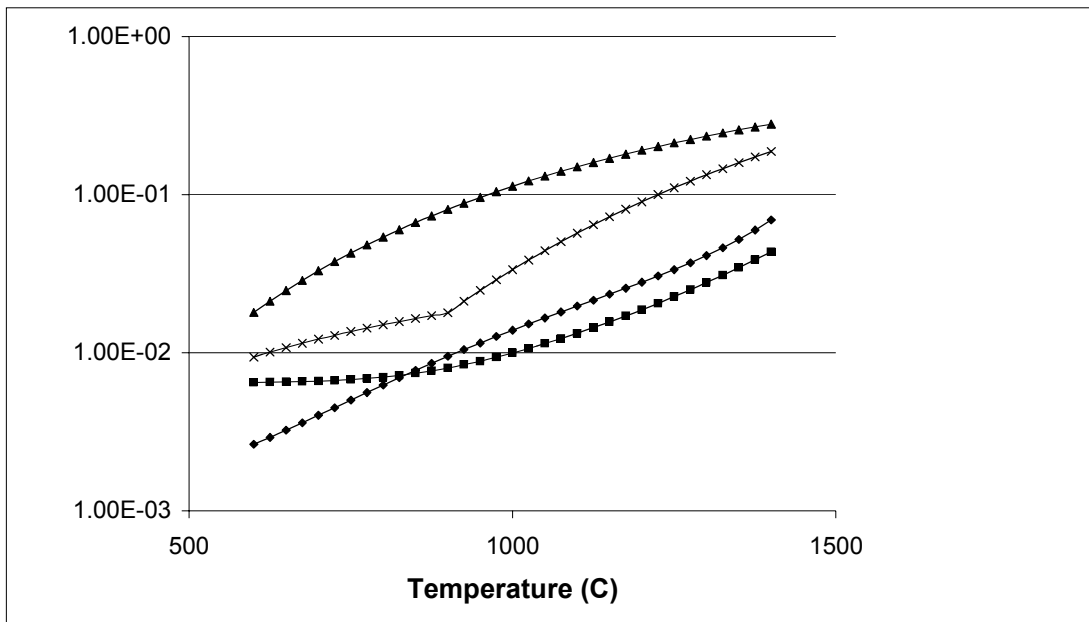


Figure 3-21 Comparison of failed particle model (R/B) results

3.7.2 Long-lived Fission Gases and Fission Metals. The release of long-lived fission gases and metals is modeled using the diffusion models presented earlier in this section using measured values for effective diffusivities for the kernel and each layer in the TRISO-coated particle. When (a fuel performance model predicts that) a given layer has failed, the release is usually calculated assuming that the failed layer offers no resistance to mass transport. This assumption is generally conservative.

It is important to consider mass transport through each layer individually since different fission products have different levels of retentiveness in each layer. For example, a particle with a failed SiC layer but intact PyC layers will release cesium but not noble gases under normal operation because the PyC layers retain noble gases up to very high temperatures. More sophisticated models that account for mass transport through a crack

or via nano-porosity as discussed earlier could also be implemented but historically have not been undertaken given the additional data needed for such mechanistic models.

3.7.3 Water and Air Ingress. In the event of water ingress, release from particles with exposed kernels has been measured (as discussed in Section 2) and some semi-empirical models exist that account for the change in release as a result of the hydrolysis of the kernel during the steam exposure. [3-2, 3-3]. In the event of air ingress, oxidation of the intact particles is considered and simple empirical models exist to predict particle failure based on experimental data [3-2]. However, modeling of the release of fission products is lacking. If a layer of the particle has been consumed in the oxidation, the modeling could conservatively assume that the layer no longer exists. For initially failed particles, the air would convert the UO_2 fuel kernel to higher oxidation states. The accompanying change in the microstructure of the kernel would increase the release.

3.8. Fission Product Transport Factors

Based on the previous sections, there is a wide range of parameters that influence fission product transport in coated particle fuel. These include:

- Parameters on the macroscopic scale such as the burnup of the particle, fast fluence (as a surrogate for radiation damage), the temperature of the layer, and the partial pressure of a gas or vapor.
- Microscopic parameters related to the structure of the material such as the porosity and tortuosity of the porous medium, and the grain boundary microstructure.
- Parameters related to the chemical speciation of the fission products of interest including the stoichiometry of the fuel and its changes during normal and accident conditions, thermochemical data such as free energies of formation, vapor pressures and adsorption isotherms, and transport properties such as binary gas phase diffusivities and heats of transport.
- Physical parameters that result in multidimensional and multicomponent effects including segregation and concentration of fission products as a result of cracking, and azimuthal temperature gradients.

To include all of these factors in the six PIRT tables were judged by the PIRT panel members and the NRC to be somewhat excessive given our state of knowledge about the importance and knowledge levels of some of the more detailed factors. As a result, a few higher level-factors were identified to account for most of the individual factors identified in this section. The factors, identified by the PIRT panel members, and their definitions, are found in Table 3-4. These factors were applied to each of the appropriate layers of the fuel from the kernel out to the fuel element (matrix materials). Not all factors are found in each layer since as discussed in the section, some of the factors may only be unique to one or two of the layers.

Table 3-4 Fission Product Transport Phenomenon Identified by the PIRT Panel

Factor	Definition
Condensed phase diffusion	Transport of condensable fission products by inter-granular diffusion and/or intra-granular solid-state diffusion (grain boundary and/or bulk diffusion)
Gas phase diffusion	Diffusion of gaseous fission products through layer (Knudsen and bulk diffusion through pore structure, and pressure driven permeation through structure including such sub-factors such as holdup, cracking, adsorption, site poisoning, permeability, sintering, and annealing)
Thermodynamics of fission product-SiC system	Chemical form of fission products including the effects of solubility, intermetallics, and chemical activity
Intercalation	Trapping of species between sheets of the graphite structure
Trapping	Adsorption of fission products on defects
Fission product release through failures, e.g., cracking	Passage of fission gas products from the buffer region through regions in the SiC layer that fail during operation or an accident

3.9 Summary

This review suggests that knowledge of the spatial and temporal temperature distribution in the reactor is an important factor for understanding fission product release from TRISO-coated particle fuels. Releases are likely to be dominated by particle failures during the accident. Thus, the source term must consider particle performance and impact of the failed particle configuration on the subsequent transport of fission products.

Different mechanisms are likely responsible for the transport of gases and metals in different layers. Gaseous transport can be described using pressure driven diffusion models through porous media but the use of these models requires information on the connected porosity, the characteristic size of the porosity and the tortuosity of the porous media, which are not well known for the layers of the TRISO coating. Metallic fission product transport is probably a combination of grain boundary and bulk diffusion depending on the temperature and specific fission product of interest.

A preliminary assessment suggests that the power generated in the particle determines conditions in the buffer (cracked versus uncracked). This in turn defines the initial conditions for fission product transport. With the exception of cracking, multi-dimensional effects may be less important. The calculations presented here suggest that Knudsen diffusion is consistent with rapid transport through the buffer and cracks but not intact PyC. Segregation/concentration of fission products at cracks can lead to greater releases and may explain some of the variability seen in accident heating tests. Thermal diffusion as a result of large thermal gradients (Soret effect) across the buffer would tend

to be most important under the cases of high power generation in the particle that leads to larger temperature gradients that typically correspond to very accelerated irradiation conditions that are not typical of gas reactors.

In all of these aforementioned calculations, the factors such as pressure driven and thermal diffusion have been examined individually. However, the literature contains many examples that indicate when all of the factors are modeled simultaneously, counterintuitive results may be obtained [3-6].

Effective diffusivities have been obtained from previous German and U.S. work, but the research did not always focus on the mechanism involved and the researchers did not always reduce the data with a specific mechanism in mind (e.g., Knudsen diffusion parameters, trapping parameters). The measured effective diffusivities in PyC and SiC are consistent with both older and more recent transport measurements. Furthermore, the aforementioned assessments suggest that trapping is important in OPyC layers where concentration of fission products is on the same order as the trap density. Trapping is much less important in IPyC and SiC layers because the trap concentration. Is expected to be much less the fission product concentration in the layers. Sensitivity studies using currently available effective diffusivities and educated guesses on trapping parameters and the simple multi-layer diffusion and trapping model presented here can help scope out these issues in more detail.

Fission product transport at the microscopic level depends strongly on the microstructure of the individual layers in the coated particle and the microstructure depends on the deposition conditions used to fabricate the layer. The understanding of the linkage between transport, microstructure and deposition conditions is not complete. Instead there is an implicit empirical relationship between the measured transport, the underlying layer structure, and the deposition conditions as implied by the measured effective diffusivities for the different layers for a specific manufactured fuel. Thus, for any new fuel that is produced, if the historical fuel fission-product-transport data are referenced, it would be important to establish that the transport-structure relationship implicit in the historic data is also applicable for the newly produced fuel. Significant deviations in the historic transport-structure relationship would raise questions about how much of the historic experimental database on fission product transport for TRISO-coated particle fuel would be valid for the new fuel that is produced.

3.10. References

- 3-1 Littmark, U., and J. F. Ziegler, "Handbook of Range Distributions for Energetic Ions in All Elements," Pergamon Press, 1980.
- 3-2 Booth, A. H., "A Method of Calculating Fission Gas Release from UO₂ Fuel and Its Implication to the X-2-f Loop Test," Atomic Energy of Canada Limited Report – 496, 1957.
- 3-3 Turnbull, J. A., et al., "The Diffusion Coefficient of Gaseous and Volatile Species During the Irradiation of Uranium Dioxide," Journal of Nuclear Materials, Vol. 107, No. 168, 1982.

-
- 3-4 Terry, W. K., (ed.), "Modular Pebble-Bed Reactor Project," Laboratory Directed Research and Development Program FY-2001 Annual Report, INEEL/EXT-2001-623, December 2001.
 - 3-5 Fuel Performance and Fission Product Behaviour in Gas Cooled Reactors, IAEA TECDOC-978, Nov. 1997.
 - 3-6 Jacox, M. E., J. Phys. Chem. Ref. Data, 32, 2003, p. 1.
 - 3-7 Bird, R. B., W. E. Stewart and E. N. Lightfoot, "Transport Phenomena," John Wiley and Sons, 1960.
 - 3-8 Toor, H. L., J. AIChE, 3 (1957) 198
 - 3-9 Shadanov, V., Yu. Kagan and A. Sazykin, Soviet Physics JETP, 15 (1962) 596.
 - 3-10 Mason, E. A., A.P. Malinauskas, and R.B. Evans III, J. Chem. Phys., 46 (1967) 3199.
 - 3-11 Jenkins, T. R. and F. Roberts, Proc. Conf. Carbon 5th, Penn State University, Vol. 2, 1961, p. 335.
 - 3-12 Kast, W., and C.-R. Hohenthanner, "Mass Transfer with the Gas-Phase of Porous Media," International Journal of Heat and Mass Transfer, Vol. 43, p. 807-823, 2000
 - 3-13 Mason, E. A., and A. P. Malinauskas, "Gas Transport in Porous Media: The Dusty Gas Model," Elsevier, Amsterdam, 1983.
 - 3-14 Hewitt, G. F., "Gaseous Mass Transport within Graphite" , Chapter 2 in Chemistry and Physics of Carbon - A Series of Advances, Volume 1, P.L. Walker, Jr., Marcel Dekker, 1965.
 - 3-15 Korte, C.; Janek, J.; Timm, H. 1997, Transport processes in temperature gradients: Thermal diffusion and Soret effect in crystalline solids. Solid State Ionics ; November, 1997; vol.101-103, no., pp. 465-470
 - 3-16 Hofman, G. L., Hayes S. L., Petri M. C. "Temperature gradient driven constituent redistribution in U-Zr alloys," Journal Of Nuclear Materials 227 (3): 277-286 Jan. 1996
 - 3-17 Kleykamp, H., 2001,"Phase equilibria in the UO_2 - PuO_2 system under a temperature gradient," Journal of Nuclear Materials; April, 2001; vol.294, no.1-2, pp. 8-12
 - 3-18 Longhurst, G. R., et al., "TMAP4 User's Manual," EGG-FSP-10315, May 1998.
 - 3-19 Petti, D. A., et al., "Key differences in the fabrication, irradiation and high temperature accident testing of US and German TRISO-coated particle fuel, and their implications on fuel performance," Nuclear Engineering and Design, Vol. 222, p. 281-297, 2003.
 - 3-20 Braun, C. et al., "Mesure de la Permeabilite aux Gaz des Revetements de Pyrocarbone Isotrope," Journal of Nuclear Materials, Vol. 89, p. 136-142, 1980.

-
- 3-21 Mathur, R. B., "In-Situ Electrical Resistivity Changes During Bromine Intercalation in Carbon Fibers," *Carbon*, Vol. 34, No. 10, pp. 1215-1220, 1996.
- 3-22 Hollerman, I., et al., "An Infrared Study on CO Intercalated in Solid C60," *J. Chem. Physics*, Vol. 110, No. 4, Jan. 1999.
- 3-23 Palnichenko, A., and S.I. Tanuma, "Effect of Intercalation of Alkali and Halogen Species into the Low Density Carbon Crystal 'Carbolite'," *J. Phys. Chem. Solids*, Vol. 57, No. 6-8, pp. 1163-1166, 1996.
- 3-24 Levi, M. D., and D. Aurbach, "Frumkin Intercalation Isotherm- a Tool for the Description of Lithium Insertion into Host Materials: A Review," *Electrochimica Acta*, Vol. 45, p. 167-185, 1999.
- 3-25 Bisquert, J., and V. S. Bikhrenko, "Analysis of the Kinetics of Ion Intercalation. Two State Model Describing the Coupling of Solid State Ion Diffusion and Ion Binding Processes," *Electrochimica Acta*, Vol. 47, p. 3977-3988, 2002.
- 3-26 Longhurst, G. R., et al., "TMAP4 User's Manual," EGG-FSP-10315, May 1998.
- 3-27 Petti, D. A., et al., "Development of Improved Models and Design of Coated Particle Gas Reactor Fuels: Annual Program Report Under the International Nuclear Energy Research Initiative (I-NERI)," INEEL/EXT-02-0493, Nov. 2002.
- 3-28 Fusamae, F., et al., "Evaluation of Grain-Boundary Groove Profiles and Surface Diffusion Coefficients in SiC Ceramics Using Atomic Force Microscopy," *Ceramic Transactions*, Vol. 71, 1996, p. 463- 472.
- 3-29 Takano, K., et al., "Volume and Dislocation Diffusion of Iron, Chromium, and Cobalt," in *CVD beta-SiC*, Science and Technology of Advanced Materials, Vol. 2 No. 2 June 2001, p. 381-388.
- 3-30 Wang, X. R., et al., "Apparent Anomalous Prefactor Enhancements for Surface Diffusion due to Surface Defects," *Surface Science*, Vol. 512, p. L361-L366, 2002.
- 3-31 Mishini, Y., and C. Herzig, "Grain Boundary Diffusion: Recent Progress and Future Research," *Materials Science and Engineering*, A260, P. 55-71, 1999.
- 3-32 Zhu, J., et al., "Microstructure Dependence of Diffusional Transport," *Computational Materials Science*, Vol. 20, p. 37-47, 2001.
- 3-33 Gyarmati, E., and H. Nickel, "Stationary and Dynamic Deposition of Silicon Carbide on Coated Fuel Particles," JUL-900-RW, ORNL-TR-2733, November 1972.
- 3-34 Gulden, T. D., "Deposition and Microstructure of Vapor-Deposited Silicon Carbide," *J. American Ceramic Society*, Vol. 51, No. 8, August 1968, p. 424-427
- 3-35 Voice, E. H., and V.C. Scott, "The Formation and Structure of Silicon Carbide Pyrolytically Deposited in a Fluidized Bed of Microspheres," *Proceedings of the 5th Symposium on Special Ceramics*, Stoke on Trent, July 14-16, 1970.

-
- 3-36 Morgan, M. T., and A. P. Malinauskas, "Cesium Release and Transport in BISO-coated Fuel Particles," Nuclear Technology, Vol. 35, p. 457-464, September 1977.
- 3-37 Olander, D. R., "Fundamental Aspects of Nuclear Reactor Fuel Elements", ERDA, TID-26711-P1, 1976.
- 3-38 Martin R. C., "Compilation of Fuel Performance and Fission Product Transport Models and Database for MHTGR Design", ORNL/NPR-91/6, October 1993.
- 3-39 Nabielek, H., "Partikeln und Brennelemente für den HTR", KFA-HTA, January 24, 1991.
- 3-40 Maki, J. T., D. A. Petti, R. R. Hobbins, R. K. McCardell, E. L. Shaber and F. H. Southworth, "NP-MHTGR Fuel Development Program Results", INEEL/EXT-2002-1268, October 2002.